


Higher-Order Null Models as a Lens for Social Systems

Giulia Preti^{1,*} Adriano Fazzino¹ Giovanni Petri^{1,2} and Gianmarco De Francisci Morales¹

¹*CENTAI Institute, Corso Inghilterra 3, 10138 Turin, Italy*

²*Network Science Institute, Northeastern University London, Devon House, 58 St. Katharine's Way, London E1W 1LP, United Kingdom*

 (Received 3 April 2024; revised 12 June 2024; accepted 9 July 2024; published 20 August 2024)

Despite the widespread adoption of higher-order mathematical structures such as hypergraphs, methodological tools for their analysis lag behind those for traditional graphs. This work addresses a critical gap in this context by proposing two microcanonical random null models for directed hypergraphs: the directed hypergraph degree model (DHDM) and the directed hypergraph JOINT model (DHJM). These models preserve essential structural properties of directed hypergraphs such as node in- and out-degree sequences and hyperedge head- and tail-size sequences, or their joint tensor. We also describe two efficient Markov chain Monte Carlo algorithms, NUDHY-DEGS and NUDHY-JOINT, to sample random hypergraphs from these ensembles. To showcase the interdisciplinary applicability of the proposed null models, we present three distinct use cases in sociology, epidemiology, and economics. First, we reveal the oscillatory behavior of increased homophily in opposition parties in the U.S. Congress over a 40-year span, emphasizing the role of higher-order structures in quantifying political group homophily. Second, we investigate a nonlinear contagion in contact hypernetworks, demonstrating that disparities between simulations and theoretical predictions can be explained by considering higher-order joint degree distributions. Last, we examine the economic complexity of countries in the global trade network, showing that local network properties preserved by NUDHY explain the main structural economic complexity indexes. This work advances the development of null models for directed hypergraphs, addressing the intricate challenges posed by their complex entity relations, and providing a versatile suite of tools for researchers across various domains.

DOI: [10.1103/PhysRevX.14.031032](https://doi.org/10.1103/PhysRevX.14.031032)

Subject Areas: Complex Systems,
Interdisciplinary Physics

I. INTRODUCTION

Higher-order mathematical structures such as hypergraphs and simplicial complexes have emerged as powerful modeling tools that overcome the limitations of traditional graph models, which by construction are restricted to binary relations between entities [1–4].

Indeed, their adoption is motivated by the observation that real-world scenarios often entail interactions among multiple entities simultaneously. Examples span systems across multiple spatial and temporal scales, including cellular processes [5,6], chemical reactions [7], protein interaction networks [8], neural processing [9,10], whole-brain activity [11,12], coauthorship networks [13,14], and contact networks [15]. Hypergraphs, in particular, are natural and flexible generalizations of graphs that model arbitrary q -ary

relations among entities. Directed hypergraphs further extend this concept by representing a link from a set of nodes (the head of the hyperedge) to another set of nodes (its tail). Consider, for instance, the case of citations among scientific publications. In this case, each citation in a publication can be modeled as a directed hyperedge from the set of authors of the publication to the set of authors of the cited work. The application of hypergraphs already spans diverse domains, from forecasting urban traffic [16] and modeling Bitcoin transactions [17] to representing web structures for accurate page reputation scoring [18] and studying the synchronization of nonlinear oscillators [19]. However, the current methodological tools for hypergraphs lag behind their counterparts in the graph world.

Understanding complex networks often involves comparing observed structures against models that mimic random scenarios. Originating from Fisher's groundwork in hypothesis testing [20], this methodology has expanded into graph theory with the study of random graph null models [21]. These models define graph ensembles that retain only selected features of the observed graph while being random in any other respect [22]. They are key tools in graph theory because they allow us to assess the

*Contact author: giulia.preti@centai.eu

Published by the American Physical Society under the terms of the [Creative Commons Attribution 4.0 International license](https://creativecommons.org/licenses/by/4.0/). Further distribution of this work must maintain attribution to the author(s) and the published article's title, journal citation, and DOI.

significance of the observed properties of real-world networks by comparing them to those obtained from randomly generated graphs [23]. This comparative analysis unveils the influence of local node features versus additional factors on network properties, and aids in identifying structural irregularities within the networks [24]. Furthermore, it enables us to assess the role of specific properties in the presence of specific empirically observed topological and structural features.

Akin to any hypothesis test, the selection of topological features to preserve in these ensembles significantly influences the conclusions drawn from the analyses. Common approaches preserve the degree sequence [25,26] and the joint degree sequence [27,28]. Random graph ensembles can be categorized into two fundamental families: microcanonical and canonical [29]. Microcanonical ensembles preserve the properties in a “hard” fashion; i.e., each of the graphs in the ensemble satisfies the imposed constraints. Conversely, canonical ensembles preserve the properties in a “soft” fashion: They maintain the constraints in expectation across the graphs in the ensemble. The choice between these approaches should be based on principled criteria, considering factors such as the characteristics of the observed data. Canonical ensembles, for instance, are better suited for scenarios where data may contain measurement errors or noise since they maintain constraints on an average basis.

Despite the vast literature on canonical and microcanonical graph ensembles [22,26,30–35], little attention has been devoted to defining null models for directed hypergraphs and developing efficient sampling algorithms for their corresponding ensembles. Existing work in the realm of hypergraphs predominantly focuses on configuration models for undirected hypergraphs [36–42], introduces max entropy models [43], or generalizes the concept of a dK-series to undirected hypergraphs [44,45].

Transitioning to developing null models for directed hypergraphs brings unique challenges due to their intricate entity relations characterized by a broader set of properties—and thus, constraints. Parameters such as the number of nodes, number of hyperedges, head- and tail-size sequences, and the frequency of nodes within hyperedge heads or tails should be taken into consideration when defining these models. Recently, Kim *et al.* [46] proposed two samplers for generating directed hypergraphs in the canonical ensemble with prescribed head- and tail-size sequences. However, due to certain design choices aimed at improving efficiency, the generated hypergraphs often exhibited structural dissimilarities from the real-world ones (see Sec. III C and Supplemental Material [47]).

This work proposes two microcanonical null models for directed hypergraphs. The first model, the directed hypergraph degree model (DHDM), preserves the in- and out-degree sequences of the nodes, as well as the head-size and tail-size sequences of the hyperedges. The second model,

called the directed hypergraph JOINT model (DHJM), preserves the joint out-in degree tensor, which encodes information about the in- and out-degree of the nodes involved in hyperedges of specific head and tail sizes. We also describe two samplers, NUDHY-DEGS and NUDHY-JOINT, to efficiently draw random hypergraphs from the corresponding ensembles. Both samplers are Markov chain Monte Carlo (MCMC) algorithms based on Metropolis-Hastings and employ targeted shuffling operations for traversal within the Markov graph.

We demonstrate the wide interdisciplinary applicability of the proposed suite of null models by showcasing three distinct use cases in sociology, epidemiology, and economics, respectively. The first one shows the role of higher-order structures in quantifying genuine political group homophily by uncovering an oscillatory behavior of increased homophily in opposition parties in the U.S. Congress across a 40-year span. The second one focuses on a nonlinear contagion in contact hypernetworks, demonstrating that the disparities observed between simulations in the hypernetworks and theoretical predictions can be explained when considering higher-order joint degree distribution, thus shedding some light on the underlying mechanisms governing these phenomena. The third and final one studies the economic complexity of countries in the global trade network and shows that the main structural economic complexity indexes [48–50] can be almost entirely explained by local properties of the network preserved by NUDHY. A more comprehensive evaluation of NUDHY with respect to other existing null models and related samplers is provided in Supplemental Material [47].

II. NULL MODELS FOR WEIGHTED DIRECTED HYPERGRAPHS

We consider weighted directed hypergraphs of the form $H \doteq (V, E)$, where $V = \{v_1, \dots, v_n\}$ is a set of nodes and $E = \{e_1, \dots, e_m\}$ is a multiset of directed hyperedges where the multiplicity of each hyperedge represents its weight. Each hyperedge $e \doteq (h, t) \in E$ consists of a head h and a tail t such that $h, t \subseteq V$. The size of e is the sum of the sizes of its head and tail $|e| = |h| + |t|$. The in-degree of a node v in H denoted as $\text{ideg}_H(v)$ is the number of tails that contain v ; the out-degree of v in H denoted as $\text{odeg}_H(v)$ is the number of heads that contain v .

A weighted directed hypergraph H can be represented, without loss of information, as a directed bipartite graph $G \doteq (L, R, D)$, where $L = V$ (left vertices), $R = E$ (right vertices), and D is a set of triplets defined as follows:

$$\begin{aligned} \forall e \doteq (h, t) \in E, \quad \forall v \in h \Rightarrow (v, e, +1) \in D, \\ \forall e \doteq (h, t) \in E, \quad \forall v \in t \Rightarrow (v, e, -1) \in D. \end{aligned}$$

For clarity, we refer to nodes when talking about the elements of the hypergraph and to vertices when talking

about the elements of the bipartite graph. Each triplet (v, e, d) is a directed edge involving a node v and a hyperedge e , where d denotes the direction of the edge: $+1$ indicates that the edge goes from a left vertex to a right vertex, whereas -1 indicates the opposite direction. We denote with \vec{D} the set of pairs of vertices connected by an edge with direction $d = +1$, i.e., $(v, \alpha) \in \vec{D} \Leftrightarrow (v, \alpha, +1) \in D$. Similarly, we denote with \overleftarrow{D} the set of pairs of vertices connected by an edge with opposite direction $d = -1$. For any vertex $v \in L$, we denote with $\overrightarrow{\Gamma}_G(v)$ the set of vertices $\alpha \in R$ such that $(v, \alpha) \in \vec{D}$, and with $\overleftarrow{\Gamma}_G(v)$ the set of vertices $\alpha \in R$ such that $(v, \alpha) \in \overleftarrow{D}$. The size of $\overrightarrow{\Gamma}_G(v)$ is called the out-degree of v , while the size of $\overleftarrow{\Gamma}_G(v)$ is the in-degree of v . Similarly, we can define the in-degree (respectively, out-degree) of a vertex $\alpha \in R$ as the size of the set of vertices $v \in L$ such that $(v, \alpha) \in \vec{D}$ [respectively, $(v, \alpha) \in \overleftarrow{D}$]. Fig. 1(a) shows an example of a directed hypergraph and the corresponding bipartite graph.

To encode the information of both the in- and out-degree of the vertices connected by the edges in G , we define the bipartite joint out-in-degree tensor (JOINT) T_G .

Definition 1 (JOINT). Let $G \doteq (L, R, D)$ be a directed bipartite graph, and $\text{IN}_L = \max_{v \in L} |\overleftarrow{\Gamma}_G(v)|$ and $\text{OUT}_L = \max_{v \in L} |\overrightarrow{\Gamma}_G(v)|$ be the largest in- or out-degree of a vertex in L , respectively. IN_R and OUT_R are similarly defined for R . The bipartite JOINT T_G of G is a five-dimensional tensor with size $\text{IN}_L + 1 \times \text{OUT}_L + 1 \times \text{IN}_R + 1 \times \text{OUT}_R + 1 \times 2$, and whose (i, j, k, l, d) th entry $T_G[i, j, k, l, d]$ for $i \in [0, \text{IN}_L]$, $j \in [0, \text{OUT}_L]$, $k \in [0, \text{IN}_R]$, $l \in [0, \text{OUT}_R]$, and $d \in \{+1, -1\}$ is the number of edges with direction d connecting a left vertex with in-degree i and out-degree j and a right vertex with in-degree k and out-degree l , i.e.,

$$T_G[i, j, k, l, d] \doteq |\{(v, \alpha, d) \in D : |\overleftarrow{\Gamma}_G(v)| = i \wedge |\overrightarrow{\Gamma}_G(v)| = j \wedge |\overleftarrow{\Gamma}_G(\alpha)| = k \wedge |\overrightarrow{\Gamma}_G(\alpha)| = l\}|.$$

A. Null model

Let \mathcal{P} be a set of properties of an observed hypergraph \hat{H} . A null model $\Pi \doteq (\mathcal{Z}, \pi)$ is a tuple where \mathcal{Z} is the set of all the hypergraphs where each P in \mathcal{P} holds (i.e., the ensemble of hypergraphs that preserve these properties), and π is a probability distribution over \mathcal{Z} .

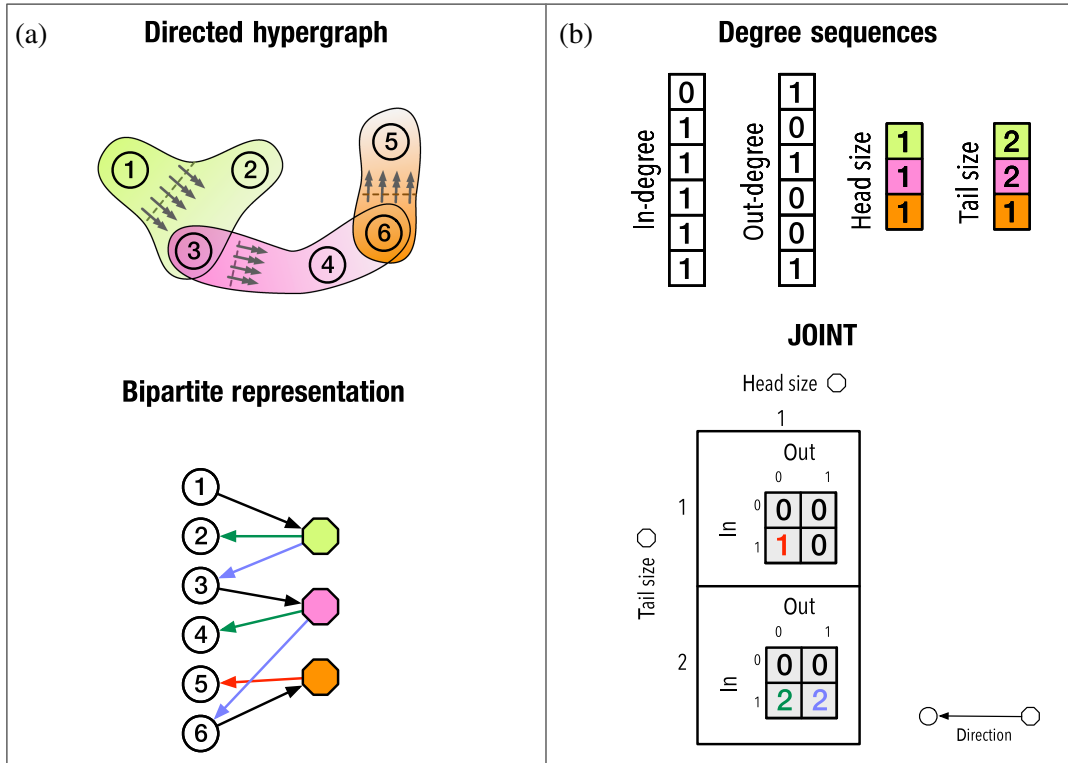


FIG. 1. Construction of directed hypergraph configuration models. (a) A directed hypergraph (top) and its representation as a bipartite graph (bottom). The left vertices (circles) correspond to hypergraph nodes, while the right vertices (hexagons) correspond to hyperedges. Dotted lines in the directed hypergraph separate the head and tail of each hyperedge, with arrows pointing toward the tail. (b) The characteristics of the observed hypergraph preserved by DHDM and DHJM: left and right in- and out-degree sequences (top) and JOINT (joint out-in-degree tensor) (bottom). The right in-degree sequence corresponds to the head-size sequence, while the right out-degree sequence corresponds to the tail-size sequence.

The first null model proposed, the DHDM and denoted as $\Pi^{\text{DHDM}} \doteq (\mathcal{Z}^{\text{DHDM}}, \pi)$, preserves the following four properties:

- P1:** head-size sequence $[|h_1|, \dots, |h_m|]$;
- P2:** tail-size sequence $[|t_1|, \dots, |t_m|]$;
- P3:** in-degree sequence $[\text{id eg}_{\hat{H}}(v_1), \dots, \text{id eg}_{\hat{H}}(v_n)]$;
- P4:** out-degree sequence $[\text{odeg}_{\hat{H}}(v_1), \dots, \text{odeg}_{\hat{H}}(v_n)]$.

Each $H \in \mathcal{Z}^{\text{DHDM}}$ has the same head-size, tail-size, in-degree, and out-degree sequences of \hat{H} . Preserving **P1** and **P2** is equivalent to preserving the sequences of the out- and in-degrees of the vertices in R in the bipartite graph representation \hat{G} of \hat{H} , and automatically preserves the sequence of the sizes of the hyperedges in \hat{H} . Preserving **P3** and **P4** corresponds to preserving the sequences of the in- and out-degrees of the vertices in L in \hat{G} , and automatically preserves the number of times each node is contained in a tail and a head of a hyperedge in \hat{H} . The in-degree, out-degree, head-size, and tail-size sequences of the directed hypergraph in Fig. 1(a) are illustrated in Fig. 1(b).

The DHDM can be regarded as a specific instance of the annotated hypergraph configuration model [51], wherein the input is a degenerate hypergraph. In these hypergraphs, each node can assume multiple roles, which in our context, manifests as a node occupying both head and tail positions within a hyperedge.

The second null model proposed, the DHJM and denoted as $\Pi^{\text{DHJM}} \doteq (\mathcal{Z}^{\text{DHJM}}, \pi)$, preserves the following property:

- P5:** JOINT $\mathbb{T}_{\hat{G}}$.

Preserving **P5** also preserves **P1–P4**.

In fact, for every $\bar{a} \in [0, \text{IN}_R]$, $\bar{b} \in [0, \text{OUT}_R]$, $\bar{c} \in [0, \text{IN}_L]$, $\bar{d} \in [0, \text{OUT}_L]$, it holds

P5 preserves **P1**:

$$|\{\alpha \in R : \text{id eg}_{\hat{H}}(\alpha) = \bar{a}\}| = 1/\bar{a} \sum_{i=0}^{\text{IN}_L} \sum_{j=0}^{\text{OUT}_L} \sum_{l=0}^{\text{OUT}_R} \mathbb{T}_{\hat{G}}[i, j, \bar{a}, l, +1]$$

P5 preserves **P2**:

$$|\{\alpha \in R : \text{odeg}_{\hat{H}}(\alpha) = \bar{b}\}| = 1/\bar{b} \sum_{i=0}^{\text{IN}_L} \sum_{j=0}^{\text{OUT}_L} \sum_{k=0}^{\text{IN}_R} \mathbb{T}_{\hat{G}}[i, j, k, \bar{b}, -1]$$

P5 preserves **P3**:

$$|\{v \in L : \text{id eg}_{\hat{H}}(v) = \bar{c}\}| = 1/\bar{c} \sum_{j=0}^{\text{OUT}_L} \sum_{k=0}^{\text{IN}_R} \sum_{l=0}^{\text{OUT}_R} \mathbb{T}_{\hat{G}}[\bar{c}, j, k, l, -1]$$

P5 preserves **P4**:

$$|\{v \in L : \text{odeg}_{\hat{H}}(v) = \bar{d}\}| = 1/\bar{d} \sum_{i=0}^{\text{IN}_L} \sum_{k=0}^{\text{IN}_R} \sum_{l=0}^{\text{OUT}_R} \mathbb{T}_{\hat{G}}[i, \bar{d}, k, l, +1]$$

To facilitate the visualization of the JOINT of the directed hypergraph in Figs. 1(a) and 1(b) illustrates a simplified representation. For each head size k and each tail

size l , it shows a two-dimensional array of size $\text{IN}_L + 1 \times \text{OUT}_L + 1$, whose (i, j) th entry indicates the number of edges with direction -1 connecting left vertices with in-degree i and out-degree j to right vertices with in-degree k and out-degree l . The $(0, 0)$ entry of each array is in the upper-left corner. In this particular example, there is only one head size (1) and two tail sizes (1 and 2). To aid comprehension, we color code the edges in the bipartite representation, matching the color of each edge to the corresponding number in the array cell it contributes to. For instance, there are two left vertices with in-degree 1 and out-degree 1 (3 and 6), each of which with one ingoing edge from a right vertex with out-degree (and thus tail size) 2. These two edges are colored in blue. Consequently, the bottom-right cell of the lower two-dimensional array contains the number 2, also colored in blue.

III. RESULTS

In this section, we present three distinct case studies that employ NUDHY-DEGS and NUDHY-JOINT, showcasing their versatility in analyzing various types of data models. While originally designed for generating random directed hypergraphs, these samplers extend their applicability to producing random undirected hypergraphs and (directed) bipartite graphs. By conceptualizing an undirected hypergraph as a directed hypergraph where heads and tails coincide, NUDHY-DEGS produces undirected hypergraphs with prescribed node degree and hyperedge size distributions, while NUDHY-JOINT produces undirected hypergraphs with prescribed joint node degree and hyperedge size distributions. Moreover, by recognizing the lossless mapping between (directed) hypergraphs and (directed) bipartite graphs, NUDHY-DEGS and NUDHY-JOINT can produce random (directed) bipartite graphs with specified left and right degree sequences, and joint degree matrices. The three case studies explore different domains, each utilizing a distinct data model. The first study delves into understanding group affinity within political parties through the analysis of sponsorship and cosponsorship relations in the U.S. Congress. We reveal nuanced patterns that evade detection when solely examining unnormalized affinity values. The second study focuses on validating a recently proposed nonlinear social contagion model for undirected hypergraphs, demonstrating how the JOINT can explain deviations from the theoretical framework in the observed data. Lastly, the third study investigates the impact of certain node properties preserved by our null models, namely, degree and joint degree distribution, on the economic competitiveness of countries measured via metrics defined for bipartite country-to-product trade networks. Here, we demonstrate that the JOINT adequately preserves rankings according to each measure of competitiveness considered. These case studies not only highlight the value of NUDHY as a lens but also yield valuable insights within

each domain, thus enriching our understanding of these complex social systems.

A. Group affinity in collaborative hypernetworks

The concept of homophily describes an individual's tendency to connect with those who share similar traits. Previous studies have consistently found this inclination across various individual features, such as gender, age, ethnicity [52], political views, and religious beliefs [53]. From its origins in sociology [54], it later became a fundamental notion in network science, because of its natural relation to the connectedness of a system. Indeed, the focus of homophily research is to grasp how these similarities among individuals shape their network of interactions [55].

Homophily can be extended to higher-order relations. Called group affinity [56], it measures the extent to which individuals in a certain class participate in groups with a certain number of individuals from the same class. It offers insights into whether participation of an individual in a group is driven by a herding behavior conditional on trait similarity.

Here, we delve into the group affinity within the Republican and Democratic parties, known as partisanship, using directed hypergraphs to represent sponsor-cosponsor relationships in Senate bills (S-BILLS) and House of Representatives bills (H-BILLS) from the 93rd to 108th Congresses [57]. We focus on bills and joint resolutions, given their potential to become law upon passage. Each bill is represented as a directed hyperedge, with the bill's sponsor (the legislator who introduced the bill) forming the head, and the set of legislators supporting the bill as cosponsors forming the tail.

In contrast to roll-call voting, where legislators must cast a vote, bill cosponsorship data offers a nuanced view of collaboration behavior as they reflect voluntary expressions of interest in supporting specific bills and reveal explicit cooperation that might not be fully captured in voting records. Thus, cosponsorship hypernetworks provide a rich account of legislative dynamics. Table II reports some statistics of the hypernetworks corresponding to each session of the Congress, for both the House and the Senate.

Formally, we study group affinity in a hypergraph $H \doteq (V, E)$ whose nodes are partitioned in a set of classes X_1, \dots, X_c . We separately consider hyperedges of the same size; i.e., we examine each subhypergraph $H^k \doteq (V, E^k \doteq \{(h, t) \in E \wedge |h| + |t| = k\})$ of H for each size k , separately. Taking inspiration from Veldt *et al.* [56], who examined how class labels affect group interactions of a fixed size k , we define a notion of the group affinity for directed hypergraphs.

For class X_i , the (α, β, k) affinity represents the extent to which a node of class X_i belongs to the tail of a hyperedge of size k where α of the β nodes in the head are from class X_i :

$$A_{\alpha, \beta, k}(X_i) = \frac{\sum_{v \in X_i} \text{ideg}_{H^k}(v, \alpha, \beta, X_i)}{\sum_{v \in X_i} \text{ideg}_{H^k}(v, \beta)}, \quad (1)$$

where $\text{ideg}_{H^k}(v, \alpha, \beta, X_i) = |\{(h, t) \in E^k : |\{u \in h \wedge u \in X_i\}| = \alpha \wedge |h| = \beta \wedge v \in t\}|$, and $\text{ideg}_{H^k}(v, \beta) = |\{(h, t) \in E^k : |h| = \beta \wedge v \in t\}|$.

To determine whether the affinity score for a certain class X_i is significantly high or low, we compare it against (i) the average score $\bar{A}_{\alpha, \beta, k}(X_i)$ measured in a collection of random hypergraphs sampled by NUDHY-DEGS and NUDHY-JOINT and (ii) a baseline score adapted from Veldt *et al.* [56]. Veldt *et al.* proposed a null probability of interactions among k nodes, with t nodes belonging to X_i . This is defined as the probability that a class- X_i node joins a group where t members are from class X_i , given that $k - 1$ other nodes are selected uniformly at random.

Similarly, our baseline (α, β, k) -affinity score for class X_i represents a null probability of k interactions with head size β :

$$B_{\alpha, \beta, k}(X_i) = \frac{\begin{matrix} [1] & [2] & [3] \\ \binom{|X_i|}{\alpha} & \binom{n - |X_i|}{\beta - \alpha} & \binom{n - 1}{k - \beta - 1} \end{matrix}}{\begin{matrix} [4] & [5] \\ \binom{n}{\beta} & \binom{n - 1}{k - \beta - 1} \end{matrix}} \quad (2)$$

$$= \frac{\binom{|X_i|}{\alpha} \binom{n - |X_i|}{\beta - \alpha}}{\binom{n}{\beta}}, \quad (3)$$

where n is the total number of nodes in H , [1] and [2] represent the number of ways to choose a head of size β with α elements of class X_i , and the remaining elements from class different from X_i , [3] represents the number of ways to choose a tail of size $k - \beta$, under the assumption that the same node can appear both in the head and in the tail of the hyperedge, having already selected one node of the tail, and [4] and [5] represent the number of ways to form a k -size hyperedge with head size β , under the assumption that the same node can appear both in the head and in the tail of the hyperedge, having already selected one node of the tail.

The specific case where the head of each hyperedge has size 1 is of particular practical interest for studying the cosponsoring of Congress bills, which are sponsored by a single member of Congress and supported by any number of cosponsors. Then, Eq. (1) reduces to

$$A_k(X_i) = \frac{\sum_{v \in X_i} \text{ideg}_{H^k}(v, X_i)}{\sum_{v \in X_i} \text{ideg}_{H^k}(v)}, \quad (4)$$

where $\text{ideg}_{H^k}(v, X_i) = |\{([u], t) \in E^k : u \in X_i \wedge v \in t\}|$. Eq. (4) can be seen as the probability that a node of class

X_i joins the tail of a hyperedge of size k , knowing that the head is of class X_i . As $\alpha = \beta = 1$, the baseline expressed by Eq. (2) reduces to

$$\mathbf{B}_k(X_i) = \frac{|X_i|}{n}. \quad (5)$$

In the case of directed hypergraphs with head sequence $[1, \dots, 1]$, we also measure the homophily \mathbf{HO} of class X_i as [58]

$$\mathbf{HO}(X_i) = \mathbf{m}(X_i)/\bar{\mathbf{m}}(X_i), \quad (6)$$

where $\mathbf{m}(X_i) = 1/|t| \sum_{\substack{e \ni (u,t) \in E \\ u \in X_i}} |\{v \in t : v \in X_i\}|$ is measured in the observed hypergraph, and $\bar{\mathbf{m}}$ is the average across the samples generated by NUDHY.

Fig. 2 illustrates the mean affinity ratios for democrats and republicans in each Congress, for S-BILLS and H-BILLS. The mean affinity ratios for NUDHY-DEGS and NUDHY-JOINT are computed by averaging the terms $\mathbf{A}_k(X_i)/\bar{\mathbf{A}}_k(X_i)$ over all hyperedge sizes $k = 2, \dots, 14$. The mean affinity ratios for Veldt *et al.* are obtained by averaging the terms $\mathbf{A}_k(X_i)/\mathbf{B}_k(X_i)$ over $k = 2, \dots, 14$. For each Congress, the background color indicates which party held the majority (shades of red for republicans and shades of blue for democrats). The intensity of color corresponds to the

size of the majority, with darker shades indicating a larger margin.

These plots show that we can draw similar conclusions when comparing the affinity values against the null models obtained by NUDHY-DEGS and NUDHY-JOINT, whereas the baseline scores offer divergent insights. The panels corresponding to NUDHY-DEGS and NUDHY-JOINT reveal a clear trend [Figs. 2(a)–2(c)]: When one party holds the majority of the seats (indicated by the corresponding color in the background), the opposing party exhibits higher group affinity. This pattern indicates a more unified front, likely in pursuit of collecting the required minimum support to pass their bills.

In instances where republicans held the majority, democrats consistently maintained a group affinity 40% to 60% higher than expected, with the exception of the 104th Congress, coinciding with the first occurrence of a republican majority in both chambers since 1953 and a government shutdown in the U.S. Conversely, during democratic majority periods, republicans exhibited notably higher group affinity, particularly leading up to the 104th session, and especially in the House. Data show a lower number of bills sponsored by republicans and a tendency to cosponsor fewer bills. However, when they decide to cosponsor a bill, it is more likely to be a bill presented by a republican. This pattern is consistent with past

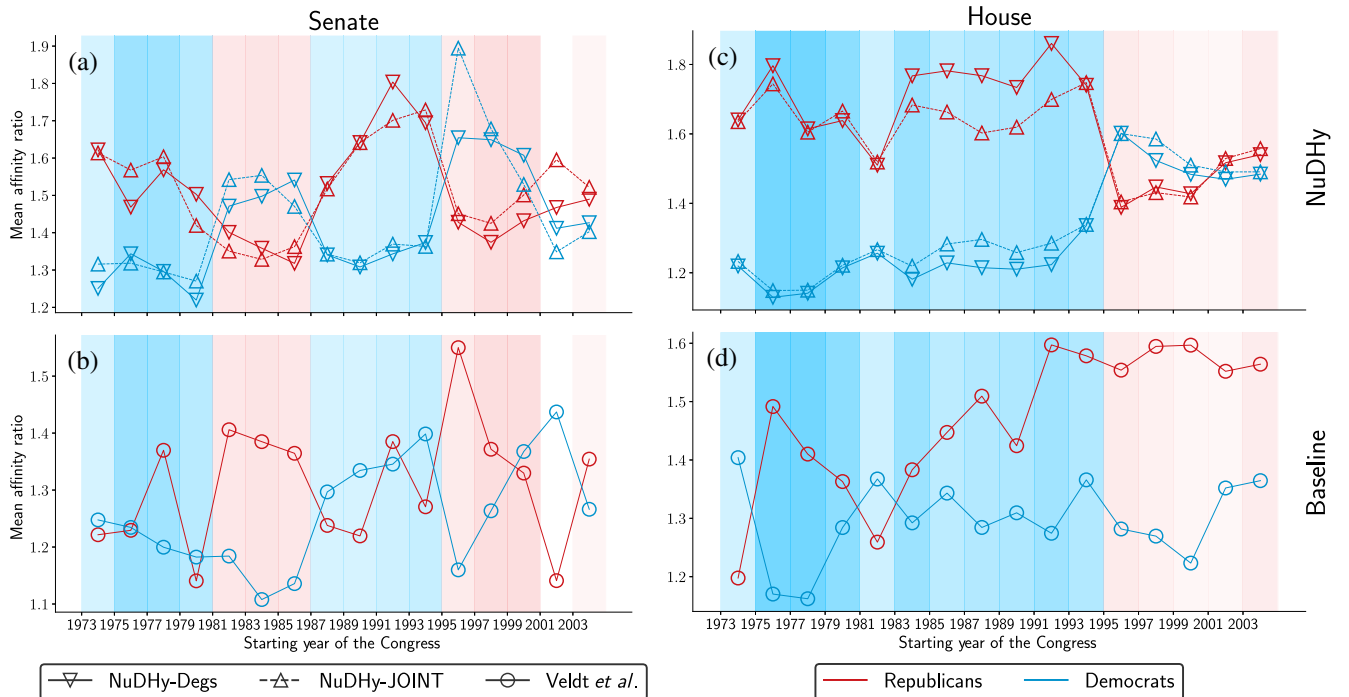


FIG. 2. Mean affinity ratios in the U.S. Congress cosponsored bills. We show results for Eq. (4) divided by the mean values in 33 samples for NUDHY-DEGS and NUDHY-JOINT for the U.S. Senate (S-BILLS) (a) and House (H-BILLS) (c). For comparison, we show the values of Eq. (4) divided by Eq. (5) for Veldt *et al.* again for the U.S. Senate (b) and House (d). The colors indicate democrats (blue) and republicans (red). We report the average ratios over $k = 2, \dots, 14$.

observations that “republicans have consistently valued doctrinal purity over pragmatic deal-making” [59].

In contrast, the baseline yields generally lower affinity values and tends to attribute higher group affinity to the Republican party, irrespective of the time period. An exception is evident in the 107th Congress starting in 2001, where the mean affinity ratio for republicans only slightly surpasses 1, whereas the ratio for democrats is roughly 1.45. During this session of the Congress, there is a discernible disparity in cosponsorship tendencies between republicans and democrats. On average, a republican member tended to cosponsor fewer bills, averaging around 119, while their democratic counterparts engaged in a higher rate of cosponsorship, averaging around 195 bills. The baseline score, which fails to consider each party’s relative prevalence and each legislator’s individual cosponsoring opportunities, inadequately acknowledges the significance of republican cosponsoring behaviors for bills sponsored by republicans versus those sponsored by democrats. Our null models, instead, maintain these characteristics of the data intact, while randomizing the rest.

In addition, we also found a clear shift in cosponsoring behavior within the House around the 104th and 105th Congresses (1995 and 1997). During this period, democrats began to consistently cosponsor a greater number of bills sponsored by democrats compared to republicans (see Table II), possibly hoping to increase the likelihood of the bills being passed. NUDHY effectively models this shift, as reflected in the corresponding mean affinity ratios.

Party homophily has been studied also by Neal *et al.* [60]. They represent bill cosponsorship data as a unipartite weighted graph, where legislators serve as nodes, and edge weights indicate the number of bills cosponsored by pairs of legislators. To ascertain statistically significant connections, they employ a stochastic degree sequence model. Despite using a data model that overlooks higher-order relations between legislators and using a simplified analytical framework (a thresholded weighted graph) [61], they find results akin to our analysis. Specifically, both studies find evidence for differential homophily: The strength of republicans’ preference for collaborating with other republicans differs from the strength of democrats’ preference for collaborating with other democrats.

Different from Neal *et al.*, our work remains faithful to the original data. Moreover, the use of randomized networks drawn from ensembles that retain some of the properties of the observed network is more suitable for identifying statistically significant connections [62].

Finally, the results concerning Eq. (6) are presented in Supplemental Material [47]. We observe that both parties exhibit an inclination toward associating with similar party members in cosponsorship relations, and that the inverse relationship between the curves of republicans and democrats remains discernible, a pattern that remains unnoticed

when solely examining the values of m measured in the observed hypergraphs.

B. Contagion processes in contact hypernetworks

The spread of information or diseases often transcends pairwise interactions and necessitates models that consider the collective influence of groups of individuals. For example, in the context of a social and behavioral contagion, multiple studies have shown that exposure to multiple sources can be required [63,64]. Models of such complex contagion processes aim to capture group influences in social phenomena, such as norm adoption, rumor spread, and disease transmission. These models embrace nonlinear connections between infection rates and sources of infection, which allows for mechanisms such as social reinforcement where multiple (or group) exposures have a larger collective impact than their sum.

More recently, multiple studies have proposed higher-order contagion models describing not only repeated interactions but rather genuine group interactions among agents. In these models, the substrates over which the process evolves are simplicial complexes [65], undirected hypergraphs [66,67], and directed hypergraphs featuring single-node tails [68]. In particular, undirected hypergraphs and simplicial complexes have proven more effective in modeling higher-order interactions between individuals. Conversely, single-tailed directed hypergraphs better model group influences on individuals. The dynamic evolution of such contagion models is typically studied numerically on real-world hypernetworks and compared to results obtained (both numerically and analytically) for the same dynamics on random hypernetworks [65,66,69]. To date, however, it is not clear what the minimal constraints are on such random hypernetworks required to reproduce the dynamical outcomes observed on the real-world hypergraphs. Here, using NUDHY, we highlight the role of structural correlations in shaping the dynamical outcomes of contagion processes. In particular, we show that stronger constraints (as implemented by NUDHY-JOINT) are required to faithfully reproduce results of superlinear contagion dynamics, while looser constraints on the degrees and tail and head sizes (NUDHY-DEGS) are sufficient when the dynamics is pairwise (linear).

We consider a hypergraph susceptible-infectious-susceptible contagion model [67] wherein the infection rate is a superlinear function of the number of infected nodes in the hyperedges. Let e be a hyperedge and i_e be the number of infected nodes in e . Then, each of the susceptible nodes in e gets infected at rate $\beta(i_e) = \lambda i_e^\nu$, where ν is a parameter to regulate the nonlinearity of the contagion process. The model assumes that infections from different hyperedges are independent processes, and thus defines the total transition rate to the infected state of a node v as the sum of the infection rates of all the hyperedges $E(v)$ containing v , i.e., $\sum_{e \in E(v)} \beta(i_e)$. Let μ denote the recovery rate (we set $\mu = 1$ in all the experiments). Nodes undergo multiple

transitions between susceptible and infected states. The contagion process is simulated using a Gillespie algorithm [70]. Starting with an initial density ρ_0 of infected nodes, the process unfolds via the two types of events (infection and recovery) occurring with probabilities proportional to their respective rates. Once a hyperedge is selected for an infection event, a susceptible node in the hyperedge is chosen uniformly at random to transition to the infected state. To obtain the density of infected nodes in the stationary state, we let the system evolve over a burn-in period $\tau_b = 10\,000$. Then, we sample $s = 10\,000$ states separated by a decorrelation period $\tau_d = 1$. Finally, we measure the mean and standard deviation of the density of infected nodes in these samples.

We compare the results of the simulations in the observed hypergraphs and the samples generated by NUDHY with the output of group-based approximate master equations (AMEs) that consider the ensemble of hypergraphs with the same distribution of hyperedge sizes and node degrees [67]. We investigate two scenarios. The first scenario involves undirected hypergraphs depicting face-to-face interactions among children in a primary school in Lyon, France [71] (LYON) and among students in a high school in Lycée Thiers, France [72] (HIGH). These hypergraphs are characterized by nearly homogeneous hyperedge size distributions (between 60% and 70% of the hyperedges have size 2, and between 15% and 20% of the

hyperedges have size 3) and bell-shaped node degree distributions centered at 11.79 and 55.63, respectively. The second scenario involves email exchanges between members of a European research institution (EMAIL-EU) and between Enron employees (EMAIL-ENRON) [73]. These hypergraphs are characterized by heterogeneous hyperedge size distributions with mean hyperedge sizes 3 and 3.42, respectively, and max hyperedge sizes 18 and 25, respectively. The node degree distributions follow a heavy-tailed distribution. The main characteristics of the four hypergraphs are reported in Table III.

Fig. 3 displays the average fraction ρ^* of infected nodes in the stationary state of contagion dynamics on the observed hypergraphs and on 33 samples generated by NUDHY-DEGS and NUDHY-JOINT, using $\rho_0 = 0.01$, and varying infection rate λ and parameter ν . The phase diagram reports also the output of the AMEs. The infection rate is rescaled with the invasion threshold λ_c , which is the minimum λ above which the healthy state ($\rho^* = 0$) is unstable. We consider both linear ($\nu = 1$) and superlinear ($\nu > 1$) contagions. In the case of linear contagions, we observe two solutions for the stationary fraction of infected nodes: $\rho_1^* = 0$ (absorbing state) and $\rho_2^* > 0$ (endemic state). For the case of superlinear contagions, we choose a value of ν greater than the bistability threshold ν_c reported in Table III. The bistability threshold is the smallest nonlinear exponent allowing for a discontinuous phase transition.

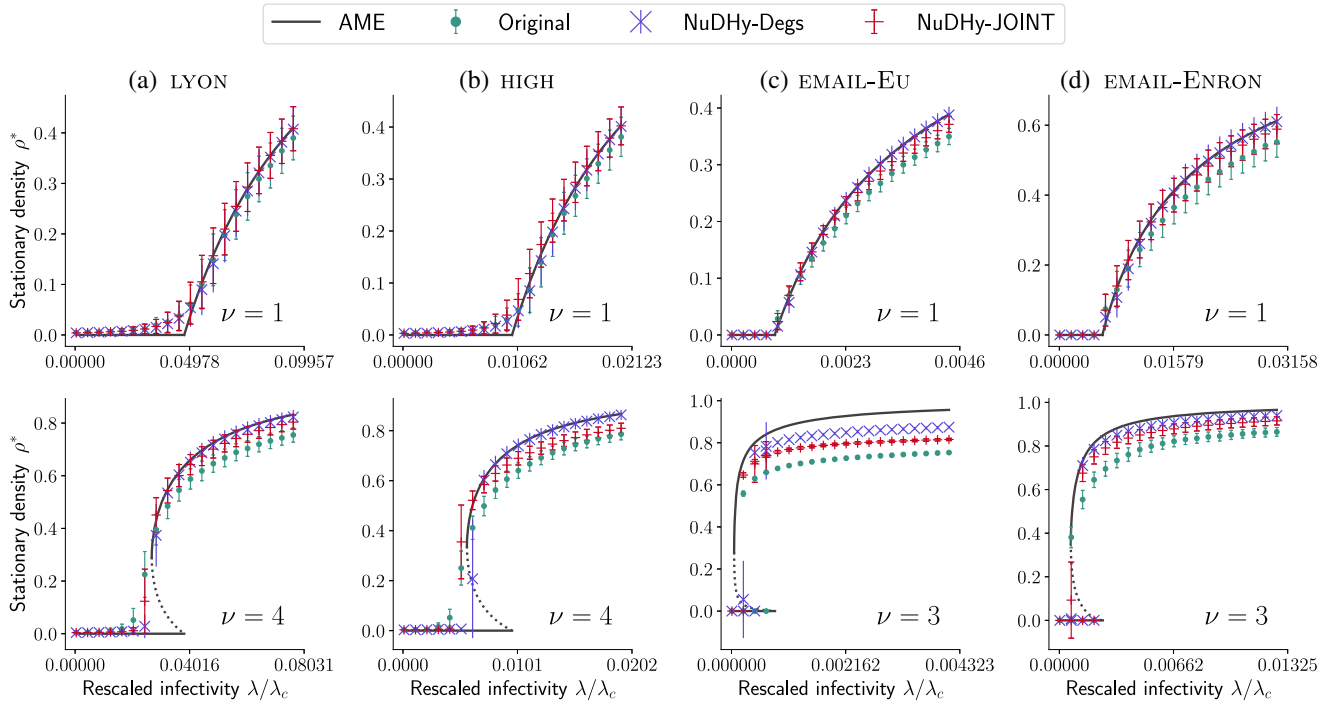


FIG. 3. Density of infected nodes in contact networks. We show the values of ρ^* in the stationary state of contagion dynamics on the observed hypergraph, and on 33 samples generated by NUDHY-DEGS and NUDHY-JOINT, varying infection rate λ and nonlinearity parameter ν , for LYON, HIGH, EMAIL-EU, and EMAIL-ENRON. We report also the output of the AMEs as defined in Ref. [67]. The infection rate is rescaled with the invasion threshold λ_c . Errors bars correspond to 1 standard deviation.

In this case, we observe three solutions: $\rho_1^* = 0$ and $\rho_3^* > 0$, which are locally stable, and $0 < \rho_2^* < \rho_3^*$, which is unstable (dashed lines). To obtain the lower branches in Figs. 3(c) and 3(d), we run the ordinary simulation method described above. On the other hand, the upper branches in Figs. 3(c) and 3(d) and the branches in Figs. 3(a) and 3(b) are obtained with a quasi-stationary-state method [74]: We keep a history of 50 past states from which a random state is used to replace the current state each time the absorbing state is reached.

Especially in the smaller datasets and for linear contagion processes, the results for NUDHY-DEGS align well with the output of the analytical framework. This is expected given that NUDHY-DEGS samples uniformly from the ensemble of hypergraphs with the same head- and tail-size sequences and the same in- and out-degree sequences, which are equivalent to the hyperedge size sequence and the node degree sequence when the input is an undirected hypergraph. The disparities observed in the superlinear processes may potentially be attributed to a too-small value assigned to τ_b .

In contrast, the structural correlations present in the observed data lead to reductions in the stationary prevalence compared to the output of the AMEs. These deviations display greater magnitude in the outputs of the superlinear contagions and in the presence of unstable regions, thus suggesting a higher influence of structural correlations within this type of contagion process. Previous works [69] have shown that the correlations are especially important in the presence of nodes with large degrees. In line with these works, we observe smaller discrepancies in LYON, where node degrees are more homogeneous. Conversely, the discrepancies in the lower branches in Figs. 3(a) and 3(b) are due to the simulations being affected by finite-size effects, while AMEs assume an infinite-size system, and they become higher for the superlinear processes.

By looking at the curves for NUDHY-JOINT in EMAIL-EU and HIGH, we observe that part of the deviation in the superlinear simulations can be explained by the joint degree distribution.

In conclusion, our analysis highlights important insights into which structure should be preserved to improve fidelity for which type of dynamical process. By comparing the results of NUDHY-JOINT with the original dynamics in the case of superlinear contagions, we observe that these dynamics can be better approximated by preserving the joint degree distributions. This is evident because the results by NUDHY-JOINT provide a better fit to the original data than those by NUDHY-DEGS. However, in the case of linear contagions, the dynamics are better represented by NUDHY-DEGS than by NUDHY-JOINT, even though NUDHY-DEGS preserves less structural information from the original hypernetwork. This demonstrates that it is not always the case that preserving more structural features leads to better fidelity.

These findings underscore the importance of carefully selecting which structural features to preserve based on the specific dynamics being studied. In particular, they

highlight the role of higher-order structural correlations in nonlinear contagion models, and thus the importance of preserving the joint degree tensor when strongly nonlinear processes or strong degree correlations are present (e.g., EMAIL-EU and HIGH).

C. Economic competitiveness in trade hypernetworks

Economic complexity metrics are indicators that aim to capture the diversity and sophistication of a country's economy through its exported product basket. The diversity and composition of a country's exported product basket, along with the complexity of the products therein, are the key properties exploited by these metrics to assess the competitiveness of countries. In this analysis, we gauge the relative economic competitiveness of countries via three of these metrics: the economic complexity index (ECI) [48], the Fitness [49,75,76], and the generalized economic complexity index (GENEPY) [50]. We apply NUDHY alongside three additional null models purposefully designed for directed hypergraphs, with the aim to investigate which characteristics of the observed data are sufficient to replicate the ranking of countries based on these metrics.

Each of the three metrics is defined on an unweighted bipartite graph that represents the export relationships between countries and products: the bipartite country-product network. The nodes of one set represent countries, and the nodes of the other set represent products. Unweighted and undirected edges connect countries with their exported products. Following previous literature in this field, we consider a country to be an exporter of a product if its revealed comparative advantage (RCA) [77] is greater than or equal to a minimum threshold R^* . RCA measures the relative monetary importance of a product for a country among the export basket of the country compared to the global average. We follow the standard economics literature and set $R^* = 1.0$ [76]. An RCA value greater than R^* implies that the given country is advanced enough to compete in the global market for that product. In addition, following the *Atlas of Economic Complexity* [78], we consider only countries with a population above 1 million and an average trade above USD 1 billion.

Let \mathbf{M} be the biadjacency matrix of the bipartite country-product network defined according to these criteria, and let \mathbf{W} be a transformation matrix defined as $\mathbf{W}[c, p] = \mathbf{M}[c, p]/k_c h_p$, where k_c is the degree of the left vertex c (representing a country), and $h_p = \sum_c \mathbf{M}[c, p]/k_c$. The country-to-country proximity matrix between countries is then defined as follows:

$$\mathbf{X}[c, c^*] = \begin{cases} \sum_p \mathbf{W}[c, p] \mathbf{W}[c^*, p] & \text{if } c \neq c^*, \\ 0 & \text{if } c = c^*. \end{cases}$$

The symmetric matrix \mathbf{X} quantifies the similarities in the export baskets of countries. Let us now recall the three metrics under study.

The ECI measures a country's complexity as the average complexity of the products it exports, and the complexity of a product as the average complexity of the countries that export it. Thus, countries with a high ECI boast diversified export portfolios, featuring unique and sophisticated products, while those with a lower ECI export a more limited selection of common goods. In terms of the biadjacency matrix \mathbf{M} , the ECI of a country and the product complexity index (PCI) of a product are defined by the following coupled equations:

$$\text{ECI}(c) = \frac{1}{\sum_p \mathbf{M}[c, p]} \sum_p \mathbf{M}[c, p] \text{PCI}(p), \quad (7)$$

$$\text{PCI}(p) = \frac{1}{\sum_c \mathbf{M}[c, p]} \sum_c \mathbf{M}[c, p] \text{ECI}(c). \quad (8)$$

The ECI index also possesses an alternative equivalent definition in terms of the eigenvector corresponding to the second largest eigenvalue of the country-to-country proximity matrix \mathbf{X} [79].

The Fitness $\mathbf{F}(c)$ of a country c and the Quality $\mathbf{Q}(p)$ of a product p are defined according to the following coupled equations [49]:

$$\begin{aligned} \tilde{\mathbf{F}}(c)^{(n)} &= \sum_p \mathbf{M}[c, p] \mathbf{Q}(p)^{(n-1)}, \\ \tilde{\mathbf{Q}}(p)^{(n)} &= \frac{1}{\sum_c \mathbf{M}[c, p] \frac{1}{\tilde{\mathbf{F}}(c)^{(n-1)}}}, \\ \mathbf{F}(c)^{(n)} &= \frac{\tilde{\mathbf{F}}(c)^{(n)}}{\langle \tilde{\mathbf{F}}(c)^{(n)} \rangle_c}, \\ \mathbf{Q}(p)^{(n)} &= \frac{\tilde{\mathbf{Q}}(p)^{(n)}}{\langle \tilde{\mathbf{Q}}(p)^{(n)} \rangle_p}, \end{aligned} \quad (9)$$

where $\langle \cdot \rangle_x$ denotes the arithmetic mean over the distribution of values for x . The main difference introduced by the Fitness and Quality scores lies in a nonlinear weighting of the fitness of the countries when computing the quality of a product rather than using a simple average. Fitness and Quality can be computed by solving Eq. (9) with an iterative algorithm, initializing $\mathbf{F}(c)^{(0)} = 1$ for each country c , and $\mathbf{Q}(p)^{(0)} = 1$ for each product p . The iterative algorithm converges to a single fixed point independent from the initial conditions [49,76,80].

Finally, the GENEPEY index is a combination of the eigenvectors of the country-to-country proximity matrix \mathbf{X} . More precisely, the GENEPEY index of a country c is defined as

$$\mathbf{G}(c) = \left(\sum_{i=1}^2 \lambda_{c,i} \mathbf{e}_{c,i} \right)^2 + 2 \sum_{i=1}^2 \lambda_{c,i}^2 \mathbf{e}_{c,i}^2, \quad (11)$$

where $\lambda_{c,i}$ is the i th largest eigenvalue of the proximity matrix \mathbf{X} , and $\mathbf{e}_{c,i}$ is the corresponding eigenvector.

As a preliminary observation, note that the bipartite country-product network inherently represents a higher-order structure [32], as any hypergraph can be represented as a bipartite graph without loss of information. Therefore, computing metrics on the bipartite country-product network corresponds to conducting higher-order analyses.

We perform a comparative analysis of country rankings based on ECI, Fitness, and GENEPEY computed from the observed data and from 33 samples generated by NUDHY. We consider international trade data for four years: 1995 (first year available), 2009 (global financial crisis), 2019 (COVID-19 outbreak), and 2020 (economic recession) [81]. We consider a directed higher-order data representation where nodes represent countries and hyperedges represent products traded by them. Coherent with the construction of the bipartite country-product network, the head of each hyperedge includes countries that export the product with a revealed comparative advantage [77] greater than 1; the tail of each hyperedge includes countries that import the product with an RCA greater than 1, and we consider only countries with a population above 1 million and an average trade above USD 1 billion. Table IV reports the characteristics of the resulting hypergraphs. This directed hypergraph encoding perfectly represents the trade data and offers opportunities for studying the system more thoroughly. For instance, while the country-product network looks only at the export side of the trades, the directed hypergraph also represents imports. Higher-order representations thus offer a richer and more detailed description of the system on which more powerful metrics can be defined (although this specific task is outside the scope of the current work).

An analysis similar to ours was presented in a previous study [82] by employing the Fitness score and the BiCM null model [32] for the bipartite country-product network. This null model maintains both the left and right degree sequences but only in expectation (canonical ensemble). The study revealed that, in general, for each country, the distribution of its ranks obtained from the samples has a mean value close to the observed rank and a wide standard deviation. We find a similar, albeit much stronger, result for NUDHY. In the following, we discuss the main findings in HS2019. The results for the other trade networks are qualitatively similar and are reported in Supplemental Material [47].

1. ECI

For NUDHY-DEGS, both the Spearman and Kendall's tau average correlation values of the rankings of countries are remarkably close to zero, and the standard deviation values for both coefficients are small (Table I). This result indicates independence between the observed ranking and the rankings provided by the samples. Fig. 4(a) (upper

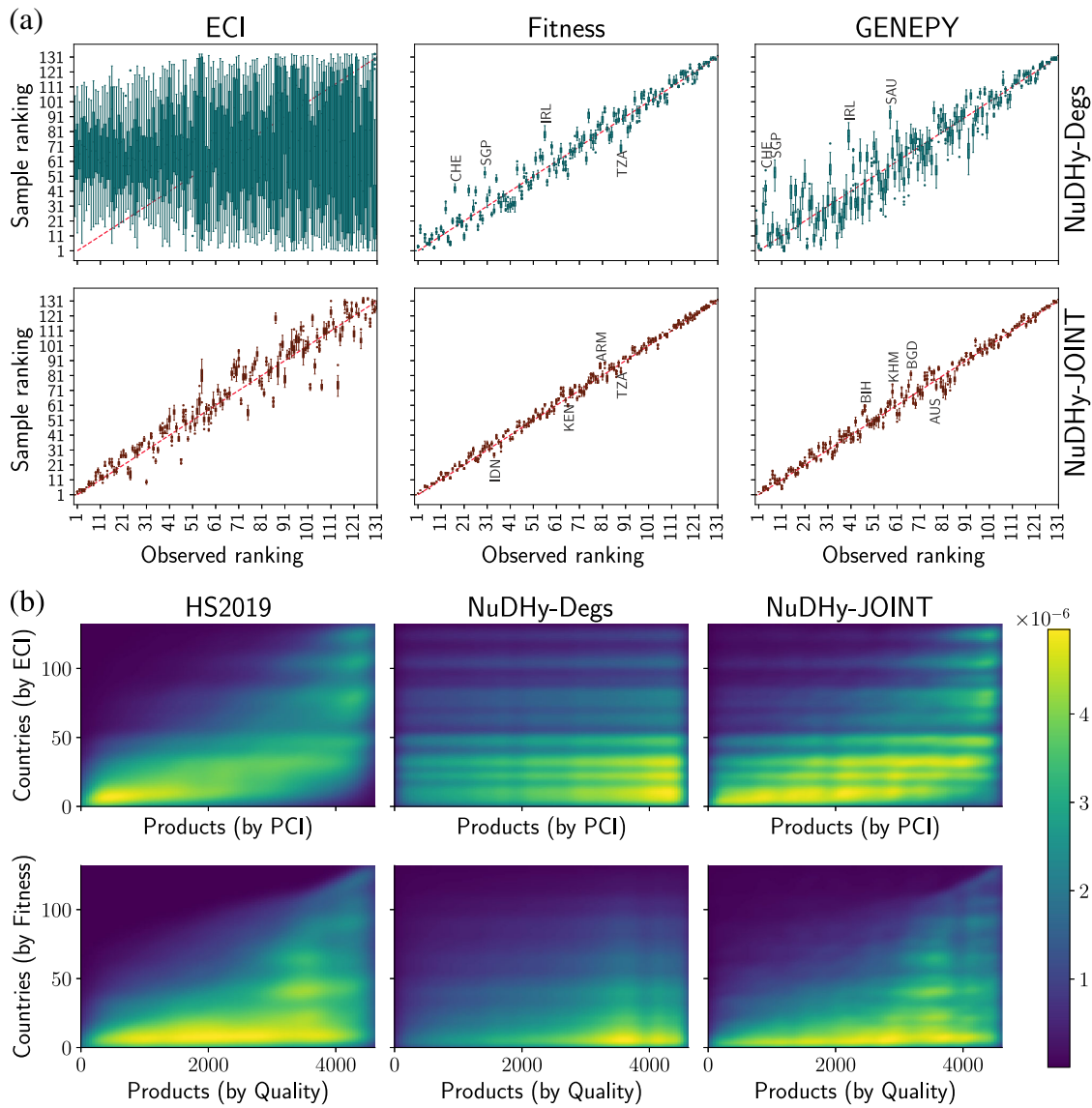


FIG. 4. Relative competitiveness in HS2019. (a) Ranking distributions based on ECI, Fitness, and GENEPEY across 33 samples for NUDHY-DEGS (top) and NUDHY-JOINT (bottom) compared to the observed rankings, with annotated top-four diverging ranks. (b) Density plots of the KDE of the observed biadjacency matrix M and of the aggregated matrices across 33 samples of NUDHY-DEGS and NUDHY-JOINT. Countries are sorted by ECI and Fitness and products by PCI and Quality (descending). The lighter the color, the higher the density of edges.

left) shows this pattern: The distributions of the ranks of each country across the samples tend to cluster around midranking positions and exhibit a wide spread, with greater variance at the lower end of the observed ranking. In other words, preserving the degrees via NUDHY-DEGS does not preserve the ECI.

In contrast, for NUDHY-JOINT both average correlation coefficients (Spearman and Kendall’s tau) of the rankings of countries are significantly high (≥ 0.84), and the standard deviation values for both coefficients are negligible (Table I). This observation suggests a dependence between the observed ranking and the rankings provided by the samples, as illustrated by the bottom left plot of Fig. 4(a).

The distributions of the ranks of each country across the samples are aligned with the observed rank of a country and present a narrow spread.

According to these results, preserving the JOINT is sufficient to preserve the ranking of countries based on their ECI score, while the degree sequence is insufficient.

2. Fitness and GENEPEY

These two measures behave quite similarly in our analysis. For NUDHY-DEGS, the average correlation coefficients (Spearman and Kendall’s tau) of the rankings of countries are significantly high for both Fitness (≥ 0.88) and

TABLE I. Average Spearman’s correlation and Kendall’s tau of the rankings of the countries based on the ECI, Fitness, and GENEPEY in 33 samples and the observed rankings, for HS2019. Standard deviations are reported in parentheses.

Score	Metric	BASE	BASED	NULL	NUDHY-DEGS	NUDHY-JOINT
ECI	Spearman	−0.144 (0.143)	−0.055 (0.120)	0.007 (0.093)	0.020 (0.121)	0.964 (0.001)
	Kendall tau	−0.092 (0.092)	−0.037 (0.079)	0.005 (0.062)	0.015 (0.082)	0.848 (0.004)
Fitness	Spearman	0.051 (0.075)	0.237 (0.055)	−0.013 (0.075)	0.981 (0.001)	0.998 (0.000)
	Kendall tau	0.034 (0.051)	0.160 (0.038)	−0.010 (0.052)	0.886 (0.003)	0.963 (0.001)
GENEPEY	Spearman	0.015 (0.078)	0.230 (0.054)	−0.002 (0.097)	0.941 (0.004)	0.993 (0.000)
	Kendall tau	0.010 (0.054)	0.156 (0.040)	−0.001 (0.040)	0.801 (0.007)	0.937 (0.002)

GENEPEY (≥ 0.8), and the standard deviation values for both coefficients are negligible (Table I). This result indicates a dependence between the observed rankings and the rankings provided by the samples. The middle and right plots of Fig. 4(a) show that the distributions of the ranks of each country across the samples tend to be close to the observed rank of a country with a narrow spread.

For NUDHY-JOINT, the average correlation coefficients (Spearman and Kendall’s tau) of the rankings of countries are even higher (≥ 0.96 for Fitness and ≥ 0.93 for GENEPEY), and the standard deviation values for both coefficients are extremely small (Table I). There is a strong dependence between the observed ranking and the rankings provided by the samples, as shown by the bottom middle and right plots of Fig. 4(a). The distributions of the country rank across the samples are aligned with the observed rank of a country, with a very limited spread.

According to these results, both the degree and joint degree sequence are sufficient to retain the ranking of countries based on their Fitness and GENEPEY scores.

Figure 4(b) displays density plots representing kernel density estimations (KDEs) of the biadjacency matrices for the country-product network of 2019. These matrices are derived from the observed data (first column) and from the aggregation of 33 samples generated by NUDHY-DEGS and NUDHY-JOINT (second and third columns). Countries and products are arranged in descending order of ECI and Fitness and PCI and Quality, respectively. The color intensity within each plot indicates the density of edges, with lighter colors indicating higher density.

As expected, countries with a high Fitness and ECI predominantly export products with high Quality and PCI, while those with lower Fitness and ECI focus solely on products with lower Quality and PCI. A comparison with the corresponding plots for NUDHY-DEGS [middle columns of Fig. 4(b)] indicates that the specialization process of countries cannot be fully explained by node degrees alone, as evidenced by the inability of NUDHY-DEGS to accurately capture the pattern observed in the real data. Conversely, plots derived from samples of NUDHY-JOINT reveal remarkably similar edge density distributions to those observed, regardless of the metrics used to sort rows and columns [first and third columns of Fig. 4(b)].

Overall, we find that preserving local properties of the hypergraph, either the degree sequences and hyperedge sizes in the case of NUDHY-DEGS or their joint tensor for NUDHY-JOINT, is sufficient to explain the rankings induced by most economic complexity measures. As a consequence, it is likely that these measures primarily capture local network structure and do not fully leverage meso- and global-scale information. Our suite of null models NUDHY can help explore the power of these structural metrics and possibly develop more comprehensive ones that can leverage the natural higher-order representation of the underlying trade data.

3. Other null models

In this experiment, we also compare our null models with three null models for directed hypergraphs named BASE, BASED, and NULL. BASE and BASED are two different versions of REDI [46]: the first realistic generative model specifically designed for directed hypergraphs. REDI extends the preferential attachment model [37] to directed hypergraphs, allowing the generation of random hypergraphs exhibiting reciprocal patterns akin to those observed in real directed hypergraphs. The random hypergraphs generated by this model preserve, on average, the distribution of head and tail sizes. The version of REDI dubbed BASE preserves, on average, the distribution of the number of hyperedges in which each group of nodes appears, while the version dubbed BASED preserves node degrees on average. NULL is a naive sampler that preserves the head- and tail-size distributions but populates the hyperedges of the random hypergraph by drawing nodes uniformly at random from the set of nodes of the observed hypergraph. We note that these generators do not account for situations where a node is related to itself and requires three input parameters: the number of nodes, a proportion β_1 of reciprocal hyperedges, and the extent β_2 of reciprocity between a hyperedge and its reciprocal counterpart. However, precise tuning of β_1 and β_2 to ensure that the reciprocity of the random samples aligns with that of the observed hypergraph is challenging due to the computational complexity of calculating reciprocity [$O(2^{|E|})$]. To circumvent this limitation, we set $\beta_1 = \beta_2 = 0$ as recommended by the authors.

NUDHY offers several key advantages over REDI. First, it preserves the degree and joint degree distributions exactly. Second, it can generate directed hypergraphs of any size, accommodating real-world scenarios where relations among large groups of nodes are common. Third, it allows nodes to belong to both the head and the tail of the same hyperedge, a flexibility that is crucial for accurately modeling certain types of hypergraphs, such as citation networks. Lastly, it is at least 1 order of magnitude faster than REDI, and thus significantly more efficient for large-scale hypergraph generation. More details on the limitations of REDI can be found in Supplemental Material [47].

According to the results reported in Table I, none among BASE, BASED, and NULL can explain the ranking of countries based on these three indexes.

IV. DISCUSSION

In this study, we introduced a suite of null models for directed hypergraphs encompassing hypergraphs with the same in-degree, out-degree, head-size, and tail-size distributions, as well as the same JOINT of an observed hypergraph. We demonstrated a lossless mapping from directed hypergraphs to directed bipartite graphs and proposed two MCMC samplers that efficiently sample from the corresponding microcanonical graph ensembles.

Our approach fills a critical gap in the existing literature, which primarily focuses on canonical and microcanonical bipartite graph ensembles [22,26,30–35] and undirected hypergraph ensembles [36–42,44,45].

We conducted rigorous experiments and evaluations, highlighting the limitations of recent generative models, such as the one proposed by Kim *et al.* [46], specifically designed for directed hypergraphs. The random hypergraphs generated by this (canonical) model preserve, on average, the distribution of head and tail sizes. However, our findings revealed structural dissimilarities between generated hypergraphs and observed ones due to design choices aimed at improving sampler efficiency.

We then showed the importance of preserving stronger structural correlations (and hence, the significance of the proposed null models) in three appropriate case studies spanning various domains. First, we explored group affinity within political parties in the U.S. Congress, revealing an inverse relationship between the affinity curves of republicans and democrats: When one party holds the majority of seats, the opposing party exhibits higher group affinity. This pattern becomes apparent only when the JOINT structural correlations are preserved.

Second, we simulated linear and nonlinear contagion processes in real and randomized hypernetworks, demonstrating the explanatory power of the JOINT in elucidating observed discrepancies between analytical contagion frameworks and simulations in real data. These results also suggest that our models could be used for more realistic data augmentation.

Third, we compared the rankings of countries based on three economic complexity indices (ECI, Fitness, and GENEPY) computed in trade hypernetworks and their randomized counterparts, highlighting the nuanced information encoded in the degree sequences and the JOINT. Our analysis revealed that both our null models accurately replicate the relative economic competitiveness of countries as measured by Fitness and GENEPY. However, for ECI, only the more restrictive null model NUDHY-JOINT succeeded in preserving the rankings. These results demonstrate that retaining the local topological properties independently is insufficient to preserve the ranking of the countries based on their ECI score. However, in all three cases, the local properties preserved by NUDHY-JOINT are sufficient to reproduce and explain the rankings, thus indicating that the metrics ignore mesoscale and global properties of the network.

Our findings emphasize the versatility and effectiveness of our proposed null models and samplers in uncovering intricate patterns across diverse disciplines. These tools represent a powerful lens through which to examine higher-order complex systems. They fill a significant gap in the analysis of higher-order networks, thus providing researchers in fields such as neuroscience, ecology, sociology, and economics with effective means for analysis and interpretation. Moreover, thanks to the efficiency of our samplers, our work empowers researchers to glean deeper insights also from more complex and larger datasets. Finally, from a theoretical perspective, our results provide direct motivation for extending analytical descriptions of hypernetworks—and of the processes taking place on them—to include more nuanced structural correlation patterns.

V. SAMPLING ALGORITHMS

This section describes two efficient sampling algorithms, NUDHY-DEGS and NUDHY-JOINT, designed for sampling from $\mathcal{Z}^{\text{DHDM}}$ and $\mathcal{Z}^{\text{DHJM}}$, respectively. Both algorithms leverage the Metropolis-Hastings algorithm as part of the Markov chain Monte Carlo approach and employ targeted edge swap operations to traverse the Markov graph. NUDHY-DEGS uses parity swap operations (Lemma 1), while NUDHY-JOINT uses restricted parity swap operations (Lemma 2). The sampling procedures for both algorithms are illustrated through pseudocode and detailed in Supplemental Material [47], together with an experimental study of their mixing time. The code is publicly available on GitHub [83].

A. NUDHY-DEGS: An efficient sampler for DHDM

We present a Markov chain Monte Carlo algorithm dubbed NUDHY-DEGS that uses Metropolis-Hastings to sample from $\mathcal{Z}^{\text{DHDM}}$ according to π . We first define an edge swap operation that transforms a bipartite graph into another bipartite graph while preserving the degree sequences and

then describe the state space that this operation induces and over which the Markov chain is constructed.

Lemma 1 (parity swap operation). Let $G \doteq (L, R, D)$ be a directed bipartite graph and $u \neq v \in L$, $\alpha \neq \beta \in R$ such that $\exists d \in \{+1, -1\}$ for which $e_1 \doteq (u, \alpha, d)$, $e_2 \doteq (v, \beta, d) \in D$ and $e_3 \doteq (u, \beta, d)$, $e_4 \doteq (v, \alpha, d) \notin D$. Swapping e_1, e_2 with e_3, e_4 generates a directed bipartite graph $G' = [L, R, (D \setminus \{e_1, e_2\}) \cup \{e_3, e_4\}]$ with the same left and right, in- and out-degree sequences as G . This swap operation denoted as $e_1, e_2 \xrightarrow{\text{PSO}} e_3, e_4$ is called a parity swap operation (PSO).

For directed unipartite graphs, this operation is known as a checkerboard swap [84]. An example of a PSO is shown in Fig. 5(a) (left).

The state space $\mathcal{G}^{\text{DHJM}}$ is a directed weighted graph. Each vertex represents a bipartite directed graph with the same left and right, in- and out-degree sequences as \hat{G} . Each edge connects two graphs that can be transformed into each other via a PSO. For any pair of graphs, there is at most one PSO that connects them; hence, there are no parallel edges between vertices. Moreover, we add self-loops from each vertex to itself. All the graphs G' that can be obtained by applying a PSO to G are called the neighbors of G in $\mathcal{G}^{\text{DHJM}}$. We associate a weight $\xi_G(G')$ to each edge (G, G')

that represents the probability of transitioning to G' starting from G .

A fundamental theorem of Markov chains states that an irreducible, aperiodic, finite Markov chain has a unique stationary distribution [85]. Therefore, the Markov chain converges to π independent of the starting state. Furthermore, we know that if the transition probability matrix is doubly stochastic, the Markov chain converges to the uniform distribution over its state space. In fact, $\pi_G = (1/n)$ is stationary for all G because $[\pi \xi_G]_G = \sum_{G'} \pi_{G'} \xi_G(G') = \sum_{G'} (1/n) \xi_G(G') = (1/n) \sum_{G'} \xi_G(G') = (1/n) = \pi_G$. As a result, samples from the chain can be considered as uniform samples from the state space. In our case, aperiodicity is guaranteed by the presence of self-loops over the vertices, while the double stochasticity of the transition matrix can be inferred from observing that (i) each PSO is reversible (i.e., if $e_1, e_2 \xrightarrow{\text{PSO}} e_3, e_4$ transforms G into G' , then $e_3, e_4 \xrightarrow{\text{PSO}} e_1, e_2$ transforms G' into G) and that (ii) the probability of going from G to G' is equal to the probability of going from G' to G , i.e., $\xi_G(G') = \xi_{G'}(G)$. The definition of ξ_G and the proof that the transition matrix $\{\xi_G(G')\}$ is doubly stochastic can be found in Supplemental Material [47], together with the proof of irreducibility. From these results, we obtain that the stationary distribution is the uniform distribution.

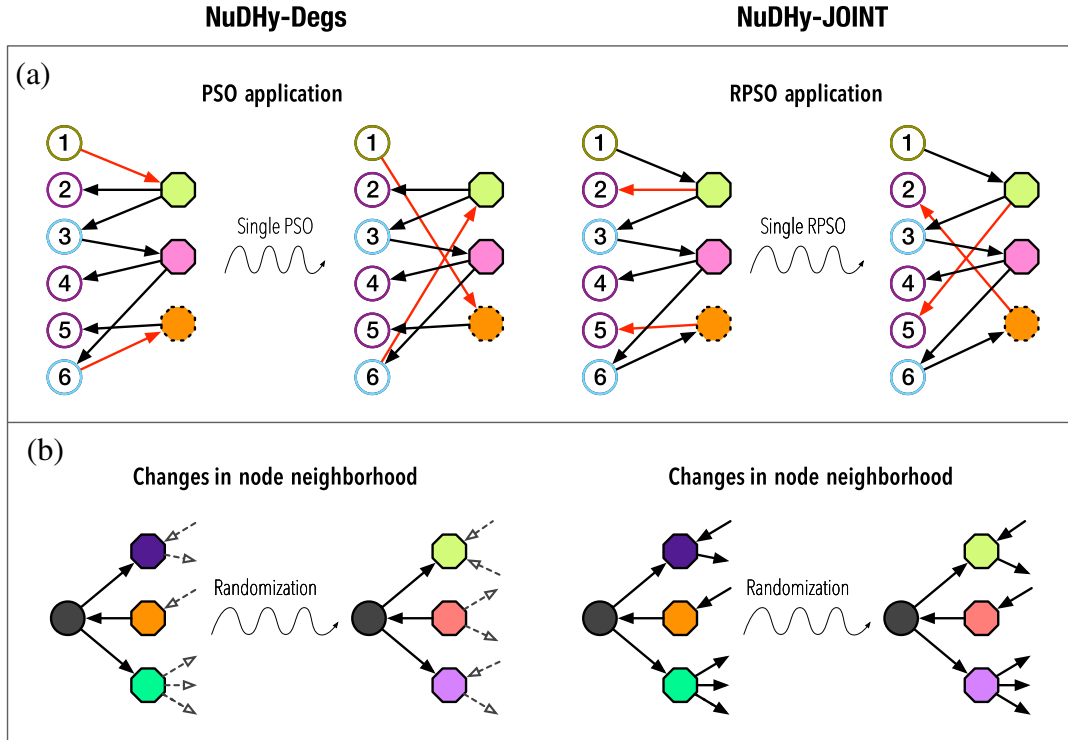


FIG. 5. (a) Bipartite graphs obtained from Fig. 1(a) after the application of the PSO (1, green hexagon, +1), (6, orange hexagon, +1) $\xrightarrow{\text{PSO}}$ (1, orange hexagon, +1), (6, green hexagon, +1), and of the RPSO (2, green hexagon, -1), (5, orange hexagon, -1), $\xrightarrow{\text{RPSO}}$ (2, orange hexagon, -1), (5, green hexagon, -1). The edges involved in the operations are highlighted in red. Left nodes with the same in- and out-degree are outlined with the same color. Right nodes with the same in- and out-degree are outlined with the same pattern. (b) Changes in the neighborhood of a left node after the application of a sequence of PSOs and of RPSOs. PSOs preserve the number of ingoing and outgoing edges of each node. RPSOs preserve also the in- and out-degree of the nodes connected to each node.

Algorithm 1: NUDHY-DEGS.

Input: Graph $G \doteq (L, R, D) \in \mathcal{G}^{\text{DHDM}}$, Number of Steps s
Output: Graph sampled uniformly from $\mathcal{G}^{\text{DHDM}}$
repeat s **times**
 out \leftarrow flip a biased coin with heads probability $|\bar{D}|/|D|$
 if out *is* heads **then**
 $u, v \leftarrow$ different vertices drawn u.a.r. from \bar{L}
 if $|X_{u,v}^+| = 0$ **then**
 continue
 else
 $\alpha, \beta \leftarrow$ pair drawn u.a.r. from $X_{u,v}^+$
 $d \leftarrow +1$
 else
 $\alpha, \beta \leftarrow$ different vertices drawn u.a.r. from \bar{R}
 if $|X_{\alpha,\beta}^+| = 0$ **then**
 continue
 else
 $u, v \leftarrow$ pair drawn u.a.r. from $X_{\alpha,\beta}^+$
 $d \leftarrow -1$
 apply $(u, \alpha, d), (v, \beta, d) \xrightarrow{\text{PSO}} (u, \beta, d), (v, \alpha, d)$ to G
return G

Algorithm 1 illustrates the sampling procedure of NUDHY-DEGS. Let $\bar{L} \doteq \{v \in L : \text{odeg}_G(v) > 0\}$ the subset of left vertices with outgoing edges, $\bar{R} \doteq \{\alpha \in R : \text{odeg}_G(\alpha) > 0\}$ the subset of right vertices with outgoing edges, and $X_{u,v}^+ \doteq \{(\alpha, \beta) : \alpha \in \bar{L}(u) \setminus \bar{L}(v) \wedge \beta \in \bar{R}(v) \setminus \bar{R}(u)\}$ be the set of pairs of out-neighbors of u and v that are not out-neighbors of v and u , respectively. The computational complexity of each step is $\Theta(\text{OUT}_L + \text{OUT}_R)$. The algorithm performs a number of steps s (input parameter) in the state space large enough that its output can be considered as a uniform sample from $\mathcal{G}^{\text{DHDM}}$. Previous works have shown that $s = O[|E| \log(|E|)]$ is, in general, sufficient [86].

B. NUDHY-JOINT: An efficient sampler for DHJM

We introduce an edge swap operation that transforms a bipartite graph into another bipartite graph with the same JOINT.

Lemma 2 (restricted parity swap operation). Let $G \doteq (L, R, D)$ be a directed bipartite graph and $u \neq v \in L$, $\alpha \neq \beta \in R$ such that $\exists d \in \{+1, -1\}$ for which $e_1 \doteq (u, \alpha, d)$, $e_2 \doteq (v, \beta, d) \in D$ and $e_3 \doteq (u, \beta, d)$, $e_4 \doteq (v, \alpha, d) \notin D$.

If $\text{iddeg}(u) = \text{iddeg}(v) \wedge \text{odeg}(u) = \text{odeg}(v) \vee \text{iddeg}(\alpha) = \text{iddeg}(\beta) \wedge \text{odeg}(\alpha) = \text{odeg}(\beta)$, then swapping e_1, e_2 with e_3, e_4 generates a directed bipartite graph $G' = [L, R, (D \setminus \{e_1, e_2\}) \cup \{e_3, e_4\}]$ with the same JOINT as G . This swap operation denoted as $e_1, e_2 \xrightarrow{\text{RPSO}} e_3, e_4$ is called a restricted parity swap operation (RPSO).

An example of an RPSO is shown in Fig. 5(a) (right).

The state space $\mathcal{G}^{\text{DHDM}}$ is a directed weighted graph where each vertex is a bipartite directed graph with the same JOINT of \hat{G} , and edges connect graphs that can be transformed into each other via an RPSO. For each pair of

Algorithm 2: NUDHY-JOINT.

Input: Graph $G \doteq (L, R, D) \in \mathcal{G}^{\text{DHJM}}$, Number of Steps s
Output: Graph sampled uniformly from $\mathcal{G}^{\text{DHJM}}$
repeat s **times**
 out \leftarrow flip a biased coin with heads prob $|\bar{D}|/|D|$
 out2 \leftarrow flip a fair coin
 if out *is* heads **and** out2 *is* heads **then**
 $i, j \leftarrow$ ints drawn with prob $\vartheta(i, j)$ from $[0, \text{IN}_L]$
 and $[1, \text{out}_L]$
 $u, v \leftarrow$ different vertices drawn u.a.r. from L_{ij}^+
 if $X_{u,v}^+ = \emptyset$ **then**
 continue
 else
 $\alpha, \beta \leftarrow$ pair drawn u.a.r. from $X_{u,v}^+$
 $d \leftarrow +1$
 else if out *is* tails **and** out2 *is* heads **then**
 $i, j \leftarrow$ ints drawn with prob $\eta(i, j)$ from $[1, \text{IN}_L]$
 and $[0, \text{out}_L]$
 $u, v \leftarrow$ different vertices drawn u.a.r. from L_{ij}^-
 if $X_{u,v}^- = \emptyset$ **then**
 continue
 else
 $\alpha, \beta \leftarrow$ pair drawn u.a.r. from $X_{u,v}^-$
 $d \leftarrow -1$
 else if out *is* heads **and** out2 *is* tails **then**
 $i, j \leftarrow$ ints drawn with prob $\phi(i, j)$ from $[1, \text{IN}_R]$
 and $[0, \text{out}_R]$
 $\alpha, \beta \leftarrow$ different vertices drawn u.a.r. from R_{ij}^-
 if $X_{\alpha,\beta}^- = \emptyset$ **then**
 continue
 else
 $u, v \leftarrow$ pair drawn u.a.r. from $X_{\alpha,\beta}^-$
 $d \leftarrow +1$
 else
 $i, j \leftarrow$ ints drawn with prob $\nu(i, j)$ from $[0, \text{IN}_R]$
 and $[1, \text{out}_R]$
 $\alpha, \beta \leftarrow$ different vertices drawn u.a.r. from R_{ij}^+
 if $X_{\alpha,\beta}^+ = \emptyset$ **then**
 continue
 else
 $u, v \leftarrow$ pair drawn u.a.r. from $X_{\alpha,\beta}^+$
 $d \leftarrow -1$
 apply $(u, \alpha, d), (v, \beta, d) \xrightarrow{\text{RPSO}} (u, \beta, d), (v, \alpha, d)$ to G
return G

vertices, there is at most one RPSO that can transform the first one into the second one, and self-loops are added to guarantee that the Markov chain is aperiodic. In Supplemental Material [47], we define a transition probability distribution ξ_G over the set of neighbors of any $G \in \mathcal{G}^{\text{DHJM}}$ and prove that $\sum_{G' \in \mathcal{G}^{\text{DHJM}}} \xi_G(G') = 1$. By observing that each RPSO is reversible and that the number of common in- and out-neighbors between any pair of nodes does not change after the application of an RPSO, we have that $\xi_G(G') = \xi_{G'}(G)$ and that the transition matrix $\{\xi_G(G')\}$ is doubly stochastic. Finally, in Supplemental Material [47] we also prove irreducibility by showing that

TABLE II. H-BILLS and S-BILLS per session: starting year, majority of seats, legislators, number of republicans (R) and of democrats (D), number of bills sponsored by republicans and democrats, mean number of bills sponsored by a republican and by a democrat, and mean number of bills cosponsored by a republican and by a democrat.

(a) House											
Start	Majority	Legislators	R	D	Bills (R)	Bills (D)	Sponsorships (R)	Sponsorships (D)	Cosponsorships (R)	Cosponsorships (D)	
93	1973	D	440	192	241	1612	3237	9.006	13.953	82.574	126.751
94	1975	D	441	144	291	1556	3927	11.358	14.385	88.231	129.823
95	1977	D	440	143	292	1758	4043	12.468	15.257	123.143	140.949
96	1979	D	438	156	276	965	2144	6.307	8.152	155.975	156.119
97	1981	D	440	191	243	1230	2017	6.543	8.732	176.933	188.984
98	1983	D	439	164	269	1023	2332	6.354	8.969	215.174	281.838
99	1985	D	438	181	252	1222	2305	6.983	9.486	241.687	318.203
100	1987	D	441	177	258	1302	2367	7.750	9.430	252.737	329.531
101	1989	D	440	174	259	1370	2660	7.874	10.391	287.596	356.031
102	1991	D	441	167	267	1323	2578	8.067	9.954	264.347	317.478
103	1993	D	441	176	258	1286	2134	7.565	8.570	226.028	223.569
104	1995	R	439	230	204	1640	1041	7.354	5.627	150.013	142.913
105	1997	R	444	226	207	1865	1294	8.216	6.811	168.740	209.708
106	1999	R	437	223	211	2176	1537	9.982	7.319	192.879	284.566
107	2001	R	442	221	211	2049	1756	9.230	8.566	170.009	298.207
108	2003	R	439	229	204	2055	1718	9.215	8.422	166.415	298.222

Senate											
Start	Majority	Legislators	R	D	Bills (R)	Bills (D)	Sponsorships (R)	Sponsorships (D)	Cosponsorships (R)	Cosponsorships (D)	
93	1973	D	101	44	54	571	1054	13.595	18.491	105.833	140.000
94	1975	D	100	37	60	526	943	14.216	15.459	101.703	101.984
95	1977	D	104	38	61	521	942	13.711	14.952	99.395	88.969
96	1979	D	101	41	58	526	866	13.150	14.931	109.927	94.797
97	1981	R	101	53	46	882	612	16.642	13.304	137.167	167.109
98	1983	R	101	54	46	1068	648	19.418	14.087	176.345	221.391
99	1985	R	101	53	46	1150	722	21.698	15.696	192.593	244.149
100	1987	D	101	45	55	770	1120	16.739	20.364	243.826	285.364
101	1989	D	100	45	55	760	1288	16.889	23.418	266.822	300.527
102	1991	D	102	44	56	722	1241	16.409	21.772	240.795	263.655
103	1993	D	101	43	57	535	985	12.159	17.589	165.091	168.228
104	1995	R	102	53	47	778	431	14.679	8.979	103.481	75.708
105	1997	R	100	55	45	912	564	16.582	12.533	123.764	126.467
106	1999	R	102	55	45	1087	822	19.411	18.267	154.036	200.543
107	2001	D	101	50	50	778	1084	15.878	21.680	119.080	195.245
108	2003	R	100	51	48	953	926	18.686	19.292	116.941	206.188

TABLE III. Contact hypernetworks: number of nodes, number of hyperedges, max hyperedge size, mean and std hyperedge size, mean and std node degree, number of steps performed by NUDHY, invasion thresholds for the linear (l) and superlinear (sl) cases, and bistability threshold.

Network	$ \mathbf{V} $	$ \mathbf{E} $	\mathbf{d}	$\mu_{ e }$	$\sigma_{ e }$	μ_{deg}	σ_{deg}	s	λ_c^l	λ_c^{sl}	ν_c
LYON	243	1188	5	2.40	0.52	11.79	5.59	57060	0.0474	0.0382	2.5415
HIGH	327	7818	5	2.33	0.53	55.63	27.06	363840	0.0101	0.0096	2.4337
EMAIL-ENRON	143	1512	18	3.00	1.95	31.82	24.22	227500	0.0060	0.0025	1.3182
EMAIL-EU	998	25027	25	3.42	2.84	85.91	114.23	1714740	0.0009	0.0008	1.2313

TABLE IV. Trade hypernetworks: number of nodes, number of hyperedges, max hyperedge size, average head size, average tail size, average node in-degree, average node out-degree, and number of steps performed by NUDHY.

Dataset	$ V $	$ E $	d	\bar{h}	\bar{t}	$\overline{\text{ideg}(v)}$	$\overline{\text{odeg}(v)}$	s
HS1995	129	5k	107	14.76	32.95	1.29k	576.3	12m
HS2009	133	4.9k	113	16.43	35.59	1.3k	604.4	13m
HS2019	133	4.6k	120	16.24	37.31	1.29k	563.9	12m
HS2020	133	4.6k	118	15.92	37.32	1.29k	552.4	12m

$\mathcal{G}^{\text{DHJM}}$ is strongly connected. From these results, we obtain that the stationary distribution is the uniform distribution.

Algorithm 2 illustrates the sampling procedure of NUDHY-JOINT. $\forall 0 \leq i \leq \text{IN}_L, 1 \leq j \leq \text{OUT}_L$, let $L_{i,j}^+ \doteq \{v \in L : \text{odeg}(v) = j \wedge \text{ideg}(v) = i\}$; $\forall 0 \leq i \leq \text{IN}_R, 1 \leq j \leq \text{OUT}_R$, let $R_{i,j}^+ \doteq \{\alpha \in R : \text{odeg}(\alpha) = j \wedge \text{ideg}(\alpha) = i\}$; $\forall 1 \leq i \leq \text{IN}_L, 0 \leq j \leq \text{OUT}_L$, let $L_{i,j}^- \doteq \{v \in L : \text{odeg}(v) = j \wedge \text{ideg}(v) = i\}$; $\forall 1 \leq i \leq \text{IN}_R, 0 \leq j \leq \text{OUT}_R$, let $R_{i,j}^- \doteq \{\alpha \in R : \text{odeg}(\alpha) = j \wedge \text{ideg}(\alpha) = i\}$; $\forall u, v \in L \cup R$, let $X_{u,v}^+ \doteq \{(\alpha, \beta) : \alpha \in \vec{\Gamma}(u) \setminus \vec{\Gamma}(v) \wedge \beta \in \vec{\Gamma}(v) \setminus \vec{\Gamma}(u)\}$, and $\forall u, v \in L \cup R$, let $X_{u,v}^- \doteq \{(\alpha, \beta) : \alpha \in \vec{\Gamma}(u) \setminus \vec{\Gamma}(v) \wedge \beta \in \vec{\Gamma}(v) \setminus \vec{\Gamma}(u)\}$. Each step takes $\mathcal{O}(\log[\max(|L|, |R|)] \times \max(\text{OUT}_L + \text{OUT}_R, \text{IN}_L + \text{IN}_R))$, and the algorithm performs a number of steps s (input parameter) large enough that its output can be considered as a uniform sample from $\mathcal{G}^{\text{DHJM}}$.

VI. DATA

We showcased the flexibility of NUDHY, considering both directed and undirected hypergraphs from various domains. All the datasets used in our analyses are publicly available on GitHub.

Table II reports the main characteristics of the directed hypergraphs representing sponsor-cosponsor relationships in Senate bills (S-BILLS) and House bills (H-BILLS) from the 93rd to 108th Congresses. We exploited these datasets in the group affinity analysis presented in Sec. III A.

Table III reports the main characteristics of the undirected hypergraphs representing (i) face-to-face interactions among children in a primary school in Lyon, France [71] (LYON) and among students in a high school in Lycée Thiers, France [72] (HIGH), and (ii) email exchanges between members of a European research institution (EMAIL-EU) and between Enron employees (EMAIL-ENRON) [73]. We exploited these datasets in the nonlinear contagion analysis presented in Sec. III B.

Table IV reports the main characteristics of the directed hypergraphs generated from international trade data [81] of four years: 1995, 2009, 2019, and 2020. The head of each hyperedge includes countries that export the product, while the tail consists of countries that import the product. We follow the standard economics literature [76] and consider

a country to be an exporter of a product if its revealed comparative advantage [77] is greater than 1, and to be an importer of a product if its revealed comparative disadvantage [87] is greater than 1. We follow Ref. [78] and include only countries with population above 1 million and average trade above USD 1 billion. We exploit these datasets in the economic complexity analysis presented in Sec. III C.

- [1] F. Battiston, G. Cencetti, I. Iacopini, V. Latora, M. Lucas, A. Patania, J.-G. Young, and G. Petri, *Networks beyond pairwise interactions: Structure and dynamics*, *Phys. Rep.* **874**, 1 (2020).
- [2] F. Battiston, E. Amico, A. Barrat, G. Bianconi, G. Ferraz de Arruda, B. Franceschiello, I. Iacopini, S. Kéfi, V. Latora, Y. Moreno *et al.*, *The physics of higher-order interactions in complex systems*, *Nat. Phys.* **17**, 1093 (2021).
- [3] C. Bick, E. Gross, H. A. Harrington, and M. T. Schaub, *What are higher-order networks?*, *SIAM Rev.* **65**, 686 (2023).
- [4] G. Gallo, G. Longo, S. Pallottino, and S. Nguyen, *Directed hypergraphs and applications*, *Discrete Appl. Math.* **42**, 177 (1993).
- [5] A. Ritz, B. Avent, and T. Murali, *Pathway analysis with signaling hypergraphs*, *Trans. Comput. Biol. Bioinform.* **14**, 1042 (2015).
- [6] S. Klamt, U.-U. Haus, and F. Theis, *Hypergraphs and cellular networks*, *PLoS Comput. Biol.* **5**, e1000385 (2009).
- [7] J. Jost and R. Mulas, *Hypergraph laplace operators for chemical reaction networks*, *Adv. Math.* **351**, 870 (2019).
- [8] S. Feng, E. Heath, B. Jefferson, C. Joslyn, H. Kvinge, H. D. Mitchell, B. Praggastis, A. J. Eisfeld, A. C. Sims, L. B. Thackray *et al.*, *Hypergraph models of biological networks to identify genes critical to pathogenic viral response*, *BMC Bioinf.* **22**, 287 (2021).
- [9] E. Schneidman, S. Still, M. J. Berry, W. Bialek, *Network information and connected correlations*, *Phys. Rev. Lett.* **91**, 238701 (2003).
- [10] E. Schneidman, M. J. Berry II, R. Segev, and W. Bialek, *Weak pairwise correlations imply strongly correlated network states in a neural population*, *Nature (London)* **440**, 1007 (2006).
- [11] C. Giusti, E. Pastalkova, C. Curto, and V. Itskov, *Clique topology reveals intrinsic geometric structure in neural correlations*, *Proc. Natl. Acad. Sci. U.S.A.* **112**, 13455 (2015).
- [12] G. Petri, P. Expert, F. Turkheimer, R. Carhart-Harris, D. Nutt, P. J. Hellyer, and F. Vaccarino, *Homological scaffolds of brain functional networks*, *J. R. Soc. Interface* **11**, 20140873 (2014).
- [13] A. Patania, G. Petri, and F. Vaccarino, *The shape of collaborations*, *EPJ Data Sci.* **6**, 18 (2017).
- [14] Q. Luo, D. Yu, Z. Cai, X. Lin, G. Wang, and X. Cheng, *Toward maintenance of hypercores in large-scale dynamic hypergraphs*, *VLDB J.* **32**, 647 (2022).
- [15] J. C. W. Billings, M. Hu, G. Lerda, A. N. Medvedev, F. Mottes, A. Onicas, A. Santoro, and G. Petri, *Simplex2vec*

- embeddings for community detection in simplicial complexes*, [arXiv:1906.09068](https://arxiv.org/abs/1906.09068).
- [16] X. Luo, J. Peng, and J. Liang, *Directed hypergraph attention network for traffic forecasting*, *IET Intell. Transp. Syst.* **16**, 85 (2022).
- [17] S. Ranshous, C. A. Joslyn, S. Kreyling, K. Nowak, N. F. Samatova, C. L. West, and S. Winters, *Exchange pattern mining in the bitcoin transaction directed hypergraph*, in *Financial Cryptography and Data Security* (2017), pp. 248–263, [10.1007/978-3-319-70278-0_16](https://doi.org/10.1007/978-3-319-70278-0_16).
- [18] K. Berlt, E. S. de Moura, A. Carvalho, M. Cristo, N. Ziviani, and T. Couto, *Modeling the web as a hypergraph to compute page reputation*, *Inf. Syst.* **35**, 530 (2010).
- [19] L. Gallo, R. Muolo, L. V. Gambuzza, V. Latora, M. Frasca, and T. Carletti, *Synchronization induced by directed higher-order interactions*, *Commun. Phys.* **5**, 263 (2022).
- [20] R. A. Fisher, *Design of experiments*, *Br. Med. J.* **1**, 554 (1936), <https://www.ncbi.nlm.nih.gov/pmc/articles/PMC2458144/>.
- [21] B. F. Manly, *A note on the analysis of species co-occurrences*, *Ecology* **76**, 1109 (1995).
- [22] T. Squartini, R. Mastrandrea, and D. Garlaschelli, *Unbiased sampling of network ensembles*, *New J. Phys.* **17**, 023052 (2015).
- [23] W. E. Schlauch and K. A. Zweig, *Influence of the null-model on motif detection*, in *Proceedings of the 2015 IEEE/ACM International Conference on Advances in Social Networks Analysis and Mining* (2015), pp. 514–519, [10.1145/2808797.2809400](https://doi.org/10.1145/2808797.2809400).
- [24] R. Fischer, J. C. Leitao, T. P. Peixoto, and E. G. Altmann, *Sampling motif-constrained ensembles of networks*, *Phys. Rev. Lett.* **115**, 188701 (2015).
- [25] N. D. Verhelst, *An efficient MCMC algorithm to sample binary matrices with fixed marginals*, *Psychometrika* **73**, 705 (2008).
- [26] G. Strona, D. Nappo, F. Boccacci, S. Fattorini, and J. San-Miguel-Ayanz, *A fast and unbiased procedure to randomize ecological binary matrices with fixed row and column totals*, *Nat. Commun.* **5**, 4114 (2014).
- [27] I. Stanton and A. Pinar, *Constructing and sampling graphs with a prescribed joint degree distribution*, *ACM J. Exp. Algorithms* **17**, 3 (2012).
- [28] M. Gjoka, B. Tillman, and A. Markopoulou, *Construction of simple graphs with a target joint degree matrix and beyond*, in *Proceedings of the 2015 IEEE Conference on Computer Communications* (2015), pp. 1553–1561, [10.1109/INFOCOM.2015.7218534](https://doi.org/10.1109/INFOCOM.2015.7218534).
- [29] G. Cimini, T. Squartini, F. Saracco, D. Garlaschelli, A. Gabrielli, and G. Caldarelli, *The statistical physics of real-world networks*, *Nat. Rev. Phys.* **1**, 58 (2019).
- [30] R. Kannan, P. Tetali, and S. Vempala, *Simple Markov-chain algorithms for generating bipartite graphs and tournaments*, *Random Struct. Algorithms* **14**, 293 (1999).
- [31] L. Tabourier, C. Roth, and J.-P. Cointet, *Generating constrained random graphs using multiple edge switches*, *ACM J. Exp. Algorithms* **16**, 1 (2011).
- [32] F. Saracco, R. Di Clemente, A. Gabrielli, and T. Squartini, *Randomizing bipartite networks: The case of the world trade web*, *Sci. Rep.* **5**, 10595 (2015).
- [33] A. A. Boroojeni, J. Dewar, T. Wu, and J. M. Hyman, *Generating bipartite networks with a prescribed joint degree distribution*, *J. Complex Netw.* **5**, 839 (2017).
- [34] S. G. Aksoy, T. G. Kolda, and A. Pinar, *Measuring and modeling bipartite graphs with community structure*, *J. Complex Netw.* **5**, 581 (2017).
- [35] C. I. Del Genio, H. Kim, Z. Toroczkai, and K. E. Bassler, *Efficient and exact sampling of simple graphs with given arbitrary degree sequence*, *PLoS One* **5**, e10012 (2010).
- [36] F. Saracco, G. Petri, R. Lambiotte, and T. Squartini, *Entropy-based random models for hypergraphs*, [arXiv:2207.12123](https://arxiv.org/abs/2207.12123).
- [37] M. T. Do, S.-e. Yoon, B. Hooi, and K. Shin, *Structural patterns and generative models of real-world hypergraphs*, in *Proceedings of the 26th ACM SIGKDD International Conference on Knowledge Discovery & Data Mining* (2020), pp. 176–186, [10.1145/3394486.3403060](https://doi.org/10.1145/3394486.3403060).
- [38] M. Barthelemy, *Class of models for random hypergraphs*, *Phys. Rev. E* **106**, 064310 (2022).
- [39] J.-L. Guo, X.-Y. Zhu, Q. Suo, and J. Forrest, *Non-uniform evolving hypergraphs and weighted evolving hypergraphs*, *Sci. Rep.* **6**, 36648 (2016).
- [40] J.-W. Wang, L.-L. Rong, Q.-H. Deng, and J.-Y. Zhang, *Evolving hypernetwork model*, *Eur. Phys. J. B* **77**, 493 (2010).
- [41] P. S. Chodrow, *Configuration models of random hypergraphs*, *J. Complex Netw.* **8**, cnaa018 (2020).
- [42] Y. Zeng, B. Liu, F. Zhou, and L. Lü, *Hyper-null models and their applications*, *Entropy* **25**, 1390 (2023).
- [43] H. Sun and G. Bianconi, *Higher-order percolation processes on multiplex hypergraphs*, *Phys. Rev. E* **104**, 034306 (2021).
- [44] K. Nakajima, K. Shudo, and N. Masuda, *Randomizing hypergraphs preserving degree correlation and local clustering*, *IEEE Trans. Netw. Sci. Eng.* **9**, 1139 (2021).
- [45] R. Miyashita, K. Nakajima, M. Fukuda, and K. Shudo, *Randomizing hypergraphs preserving two-mode clustering coefficient*, in *Proceedings of the IEEE International Conference on Big Data and Smart Computing* (2023), pp. 316–317, [10.1007/978-3-031-39831-5_18](https://doi.org/10.1007/978-3-031-39831-5_18).
- [46] S. Kim, M. Choe, J. Yoo, and K. Shin, *Reciprocity in directed hypergraphs: Measures, findings, and generators*, *Data Min. Knowl. Discov.* **37**, 2330 (2023).
- [47] See Supplemental Material at <http://link.aps.org/supplemental/10.1103/PhysRevX.14.031032> for proofs of the correctness of the algorithms and additional experiments.
- [48] C. A. Hidalgo, B. Klinger, A.-L. Barabási, and R. Hausmann, *The product space conditions the development of nations*, *Science* **317**, 482 (2007).
- [49] A. Tacchella, M. Cristelli, G. Caldarelli, A. Gabrielli, and L. Pietronero, *A new metrics for countries' fitness and products' complexity*, *Sci. Rep.* **2** (2012).
- [50] C. Sciarra, G. Chiarotti, L. Ridolfi, and F. Laio, *Reconciling contrasting views on economic complexity*, *Nat. Commun.* **11**, 3352 (2020).
- [51] P. Chodrow and A. Mellor, *Annotated hypergraphs: models and applications*, *Appl. Netw. Sci.* **5**, 1 (2020).
- [52] J. Moody, *Race, school integration, and friendship segregation in America*, *Am. J. Sociology* **107**, 679 (2001).

- [53] C. P. Loomis, *Political and occupational cleavages in a Hanoverian village, Germany: A sociometric study*, *Sociometry* **9**, 316 (1946).
- [54] P. F. Lazarsfeld and R. K. Merton, *Friendship as a social process: A substantive and methodological analysis*, *Freedom Control Mod. Soc.* **18**, 18 (1954), <https://api.semanticscholar.org/CorpusID:140840153>, <https://lccn.loc.gov/54007534>.
- [55] M. McPherson, L. Smith-Lovin, and J. M. Cook, *Birds of a feather: Homophily in social networks*, *Annu. Rev. Sociol.* **27**, 415 (2001).
- [56] N. Veldt, A. R. Benson, and J. Kleinberg, *Combinatorial characterizations and impossibilities for higher-order homophily*, *Sci. Adv.* **9**, eabq3200 (2023).
- [57] J. H. Fowler, *Legislative cosponsorship networks in the U.S. House and Senate*, *Soc. Networks* **28**, 454 (2006).
- [58] J. Park and A.-L. Barabási, *Distribution of node characteristics in complex networks*, *Proc. Natl. Acad. Sci. U.S.A.* **104**, 17916 (2007).
- [59] M. Grossmann and D. A. Hopkins, *Ideological republicans and group interest democrats: The asymmetry of American party politics*, *Perspect. Politics* **13**, 119 (2015).
- [60] Z. P. Neal, R. Domagalski, and X. Yan, *Homophily in collaborations among U.S. House Representatives, 1981–2018*, *Soc. Networks* **68**, 97 (2022).
- [61] L. Peel, T. P. Peixoto, and M. De Domenico, *Statistical inference links data and theory in network science*, *Nat. Commun.* **13**, 6794 (2022).
- [62] L. Röttjers, D. Vandeputte, J. Raes, and K. Faust, *Null-model-based network comparison reveals core associations*, *ISME Commun.* **1**, 36 (2021).
- [63] B. Mønsted, P. Sapiezynski, E. Ferrara, and S. Lehmann, *Evidence of complex contagion of information in social media: An experiment using Twitter bots*, *PLoS One* **12**, e0184148 (2017).
- [64] M. Karsai, G. Iniguez, K. Kaski, and J. Kertész, *Complex contagion process in spreading of online innovation*, *J. R. Soc. Interface* **11**, 20140694 (2014).
- [65] I. Iacopini, G. Petri, A. Barrat, and V. Latora, *Simplicial models of social contagion*, *Nat. Commun.* **10**, 2485 (2019).
- [66] G. F. de Arruda, G. Petri, and Y. Moreno, *Social contagion models on hypergraphs*, *Phys. Rev. Res.* **2**, 023032 (2020).
- [67] G. St-Onge, I. Iacopini, V. Latora, A. Barrat, G. Petri, A. Allard, and L. Hébert-Dufresne, *Influential groups for seeding and sustaining nonlinear contagion in heterogeneous hypergraphs*, *Commun. Phys.* **5**, 25 (2022).
- [68] S. Cui, F. Liu, H. Jardón-Kojakhmetov, and M. Cao, *General SIS diffusion process with indirect spreading pathways on a hypergraph*, [arXiv:2306.00619](https://arxiv.org/abs/2306.00619).
- [69] G. St-Onge, H. Sun, A. Allard, L. Hébert-Dufresne, and G. Bianconi, *Universal nonlinear infection kernel from heterogeneous exposure on higher-order networks*, *Phys. Rev. Lett.* **127**, 158301 (2021).
- [70] D. T. Gillespie, *Stochastic simulation of chemical kinetics*, *Annu. Rev. Phys. Chem.* **58**, 35 (2007).
- [71] V. Gemmetto, A. Barrat, and C. Cattuto, *Mitigation of infectious disease at school: Targeted class closure vs school closure*, *BMC Infect. Dis.* **14**, 695 (2014).
- [72] R. Mastrandrea, J. Fournet, and A. Barrat, *Contact patterns in a high school: A comparison between data collected using wearable sensors, contact diaries and friendship surveys*, *PLoS One* **10**, e0136497 (2015).
- [73] A. R. Benson, R. Abebe, M. T. Schaub, A. Jadbabaie, and J. Kleinberg, *Simplicial closure and higher-order link prediction*, *Proc. Natl. Acad. Sci. U.S.A.* **115**, E11221 (2018).
- [74] M. M. de Oliveira and R. Dickman, *How to simulate the quasistationary state*, *Phys. Rev. E* **71**, 016129 (2005).
- [75] A. Tacchella, M. Cristelli, G. Caldarelli, A. Gabrielli, and L. Pietronero, *Economic complexity: Conceptual grounding of a new metrics for global competitiveness*, *J. Econ. Dyn. Control* **37**, 1683 (2013).
- [76] M. Cristelli, A. Gabrielli, A. Tacchella, G. Caldarelli, and L. Pietronero, *Measuring the intangibles: A metrics for the economic complexity of countries and products*, *PLoS One* **8**, e70726 (2013).
- [77] B. Balassa, *Trade liberalisation and “revealed” comparative advantage*, *Manch. Sch.* **33**, 99 (1965).
- [78] H. G. Lab, *Atlas complexity ranking*, <https://atlas.cid.harvard.edu/rankings>.
- [79] S. Inoua, *A simple measure of economic complexity*, *Res. Policy* **52**, 104793 (2023).
- [80] E. Pugliese, A. Zaccaria, and L. Pietronero, *On the convergence of the fitness-complexity algorithm*, *Eur. Phys. J. Special Topics* **225**, 1893 (2016).
- [81] R. Hausmann, C. A. Hidalgo, S. Bustos, M. Coscia, and A. Simoes, *The Atlas of Economic Complexity: Mapping Paths to Prosperity* (MIT Press, Cambridge, MA, 2014).
- [82] M. J. Straka, G. Caldarelli, T. Squartini, and F. Saracco, *From ecology to finance (and back?): A review on entropy-based null models for the analysis of bipartite networks*, *J. Stat. Phys.* **173**, 1252 (2018).
- [83] G. Preti, A. Fazzino, G. Petri, and G. De Francisci Morales, *Null models for directed hypergraphs* (2024), <https://github.com/lady-bluecopper/NuDHu>.
- [84] Y. Artzy-Randrup and L. Stone, *Generating uniformly distributed random networks*, *Phys. Rev. E* **72**, 056708 (2005).
- [85] A. S. S. Rao and C. R. Rao, *Principles and Methods for Data Science* (Elsevier, New York, 2020).
- [86] F. Viger and M. Latapy, *Efficient and simple generation of random simple connected graphs with prescribed degree sequence*, *J. Complex Netw.* **4**, 15 (2016).
- [87] P. R. Krugman and M. Obstfeld, *International Economics: Theory and Policy* (Pearson Education, London, 2009).